AUTOMATIC BLEEDING DETECTION SCHEME BASED ON SPATIO-TEMPORAL FEATURE EXTRACTION FROM WIRELESS CAPSULE ENDOSCOPY VIDEOS

by

Tonmoy Ghosh

MASTER OF SCIENCE IN ELECTRICAL AND ELECTRONIC ENGINEERING

Department of Electrical and Electronic Engineering
BANGLADESH UNIVERSITY OF ENGINEERING AND TECHNOLOGY

April 2016

The thesis entitled **"AUTOMATIC BLEEDING DETECTION SCHEME BASED ON SPATIO-TEMPORAL FEATURE EXTRACTION FROM WIRELESS CAPSULE ENDOSCOPY VIDEOS "** submitted by Tonmoy Ghosh, Student No.: 0412062212F, Session: April, 2012 has been accepted as satisfactory in partial fulfillment of the requirement for the degree of MASTER OF SCIENCE IN ELECTRICAL AND ELECTRONIC ENGINEERING on April 02, 2016.

BOARD OF EXAMINERS

1. _____

(Dr. Shaikh Anowarul Fattah) **Chairman**
Professor (Supervisor)
Department of Electrical and Electronic Engineering
Bangladesh University of Engineering and Technology
Dhaka - 1000, Bangladesh.

2. _____

(Dr. Taifur Ahmed Chowdhury) **Member**
Professor and Head (Ex-officio)
Department of Electrical and Electronic Engineering
Bangladesh University of Engineering and Technology
Dhaka - 1000, Bangladesh.

3. _____

(Dr. Mohammed Imamul Hassan Bhuiyan) **Member**
Professor
Department of Electrical and Electronic Engineering
Bangladesh University of Engineering and Technology
Dhaka - 1000, Bangladesh.

4. _____

(Dr. Mohammad Rakibul Islam) **Member**
Professor (External)
Department of Electrical and Electronic Engineering
Islamic University of Technology (IUT), Bangladesh
Board Bazar, Gazipur-1704, Bangladesh.

CANDIDATE'S DECLARATION

I, do, hereby declare that neither this thesis nor any part of it has been submitted elsewhere for the award of any degree or diploma.

Signature of the Candidate

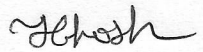

Tonmoy Ghosh

Dedication

To my parents.

Acknowledgments

I would like to express my unbound respect and thankfulness to my supervisor Dr. Shaikh Anowarul Fattah for his proper guidance and support during the span of this research. I worked under his supervision even during my undergraduate studies. My interest towards research first flourished in the final year of the undergraduate program, whilst I went to work for him. It was him who motivated me to incite my own aptitude for knowing the unknown, encouraged me to the utmost and gave rise to the confidence in me that in an underdeveloped country like ours; it is possible to conduct research of superior quality even at the undergraduate level. He not only acted as my supervisor but also helped me take important decisions of my academic career. Among many things I learned from Dr. Fattah, perseverance and constant hard work are the keys to open doors of solutions for several important issues in the area of bleeding detection in wireless capsule endoscopy. I believe our work in the past one year advanced the state of the art of the bleeding detection and classification problem. I also want to thank him for affording so much time for me in exploring new areas of my research and new ideas and improving the writing of this dissertation. After him, I would like to express my sincere gratitude towards Dr. M. G. Kibria and Dr. S. N. F. Rumi of Dhaka Medical College and Hospital, helps us providing the ground truth of bleeding image and zone. Then, I would also like to thank the rest of the members of my thesis committee: Prof. Dr. Taifur Ahmed Chowdhury, Prof. Dr. Mohammed Imamul Hassan Bhuiyan, and Prof. Dr. Mohammad Rakibul Islam, for their encouragement and insightful comments. I would like to thank the head of the department of Electrical and Electronic Engineering for allowing me to use the lab facilities, which contributed greatly in completing the work in time. I wish to give special thanks to Dr. Celia Shahnaz, for providing inspiration and guidance to walk the right path of research to success during not only MS studies but also the whole span of my research life in BUET. And most importantly, I wish to thank my parents, without whose prayers and constant support, I could never reach this stage of my life.

Abstract

Wireless capsule endoscopy (WCE) is the most advanced and non-invasive video technology to detect small intestine diseases, such as bleeding. Recently, automatic bleeding detection methods have received much attention by several researchers because of its huge diagnostic demand. In this research, efficient bleeding detection schemes are developed to detect bleeding frames and zones in WCE video. In order to detect bleeding frames, both image-based and block-based feature extraction methods are investigated. In the image-based method, instead of using conventional color spaces, a composite color plane is introduced and various statistical features are computed in that plane. One major advantage of this method is its low computational burden. However, the detection performance strongly depends on the amount of bleeding zones. Next, a color histogram based feature extraction method is proposed for block-based analysis where block statistical features are utilized. Here the effect of number of histogram bins, block size and amount of block overlap on overall performance is investigated. In order to use the advantages of both block-based and region-based method, a cluster specific feature extraction method is proposed, which introduces an unsupervised clustering step to segment the image into two classes prior to global feature extraction. It is found that instead of extracting features from the entire image if features from each cluster along with the differential cluster features are used significantly better detection performance can be achieved. For the purpose of classification, various classifiers have been tested, such as support vector machine, k-nearest neighbor and linear discriminant analysis. Once a bleeding image is detected in a WCE video, automatic marking of the bleeding zone is very much supportive for the reviewer to diagnose the diseases. Thus, in this research, based on the features extracted for frame classification, bleeding zone detection schemes are also developed. Finally, in order to continuously track bleeding frames in a WCE video, a post-processing algorithm is introduced considering the decisions made on neighboring frames. Extensive experimentation is carried out on several WCE videos and a very satisfactory performance in comparison to some of the recent methods is achieved in terms of accuracy, sensitivity, and specificity for both bleeding frame and zone detection.

Contents

List of Tables

List of Figures

Chapter 1

Introduction

In this chapter, a brief description of some computer aided method of automatic bleeding detection in wireless capsule endoscopy (WCE) is presented. It begins with a brief introduction to the WCE technology and its scope in the diagnosis of bleeding related abnormalities. The motivation behind the use of block-based classification technique is its ability to utilize information from the local regions of the video frames. The limited exploration of this technique in the existing works related to bleeding detection has also provided a motivation for investigating the approach in this field. The chapter presents the motivation of the thesis by providing the past and current research scenarios in the use of various types of feature extraction and classification techniques. The objectives and organization of the thesis are finally presented at the end.

1.1 Background

Since the discovery of fiber-optic endoscopy to examine upper and lower gastrointestinal tract, diagnosis and therapy of gastrointestinal diseases were revolutionized. However, using this type of endoscopy, in the small bowel, only the proximal duodenum, and distal ileum can be examined. Rest of the small bowel, which is more than four meters in length, remained like a black box. With the discovery of capsule endoscopy in 2000 [2], not only the small bowel became visible to the Gastroenterologist but also it led to the discovery of a new technology by which a swallowed capsule could take images of the gastrointestinal track and send these to a computer using the radio-frequency transmitter. The value, safety, and acceptability of this technology are further documented by the fact that within a year of its discovery,

it was approved by US food and drug administration (FDA) [3]. Later on, it has been proven to be the best choice of investigation for visualizing the entire small bowel [4]. These led to an era of physiological endoscopy, the scope of which is now increasing day by day to include colon and esophageal capsule endoscopy, steerable capsule and therapeutic capsule endoscopy.

1.2 Wireless Capsule Endoscopy

Wireless capsule endoscopy (WCE), also called video capsule endoscopy (VCE) or simply capsule endoscopy (CE) is a unique endoscopic technique which was first developed by Given Imaging [2]. It uses a different approach for examining of the GI tract than the thin lighted tube approach where a tube is inserted down the throat. Though the standard endoscopic techniques are able to perform both diagnostic and limited therapeutic functions, these techniques are painful and uncomfortable to the patients. WCE technology was thus developed as an innovative way to perform a non-invasive examination of the GI tract. This technique employs a pill-shaped miniaturized device which captures and transmits the images from the interior of the GI tract of the patients. Over subsequent years, CE systems from other manufacturers also entered the commercial market. Currently, three WCE systems are approved by the FDA for the diagnosis of the small bowel: PillCam SB2 by Given Imaging Ltd, Israel; Endocapsule by Olympus America Inc., Pennsylvania; and MicroCam by IntroMedic Company Ltd, Korea [3]. PillCam Colon of the Given Imaging has also been recently cleared by the FDA for the visualization of the colon [5]. Given Imaging has also developed CE systems for the visualizing esophagus. Capsule endoscopy is used for the investigation of various small bowel diseases, such as obscure gastrointestinal bleeding, celiac disease and other types of mal-absorption syndrome, polyposis, Crohn disease, ulcer, tumor etc. Image of different indications is presented in Fig. 1.1, where tuberculosis, tumors, hookworm and bleeding symptoms are illustrated. Colon capsule and esophageal capsules are used for esophageal and colonic diseases [6].

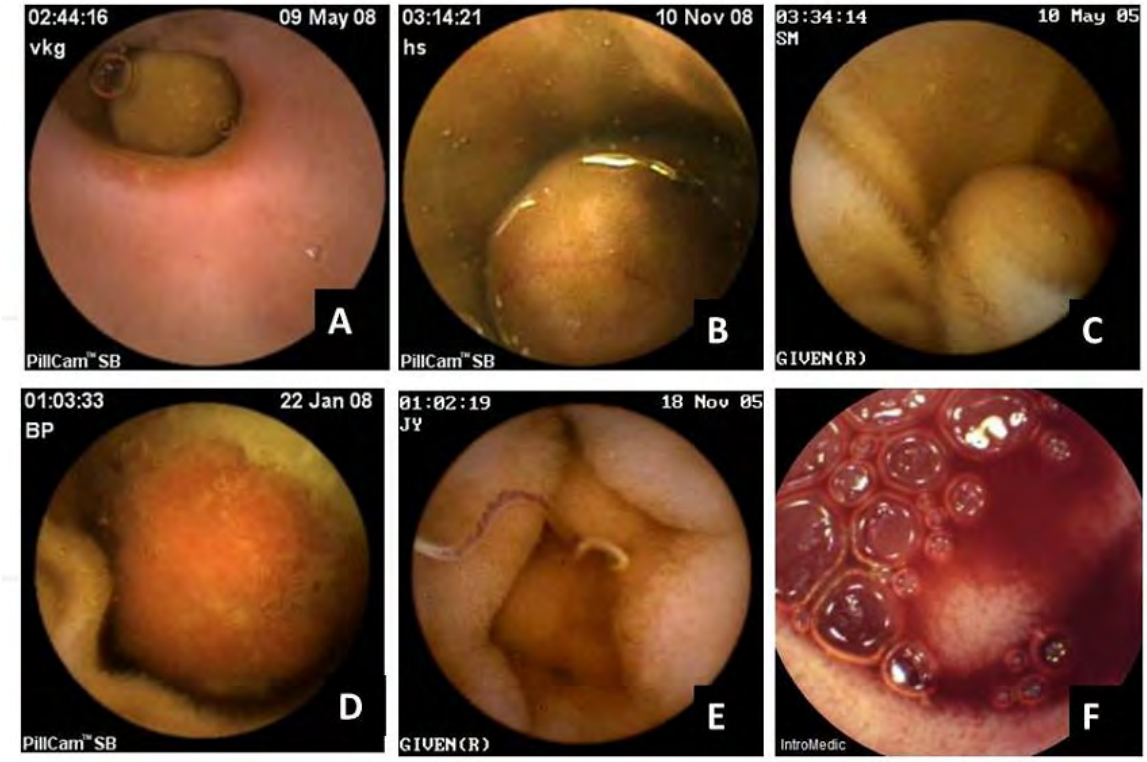

Fig. 1.1: Representative capture images of WCE for different cases, (A) tuberculosis with enterolith, (B, C, D) small bowel tumors, (E) hookworm, and (F) active bleeding; source: [1]

1.2.1 Wireless Capsule Endoscopy System

The WCE system consists of four components: 1) capsule, 2) sensor array, 3) real-time viewer and 4) computer with relevant software. All the four components along with a schematic representation of parts of capsule and sensor location guide in the patient body are illustrated in Fig. 1.2. Most capsules consist of a lens, 4 light emitting diodes, a color camera, 2 batteries, a radio-frequency transmitter and an antenna (Fig. 1.2) [7]. The camera transmits multiple (usually 2 frames per second) images by radio-frequency through the sensor to a recorder. The specification of 'Pillcam SB2' capsule is listed in Table. 1.1. A patient can swallow capsule due to its small size (26 mm in length). Before patient swallows the capsule, 8 skin antennas are taped to the anterior abdominal wall (Fig. 1.2). The capsule, while moving inside gastrointestinal tract, takes images and sends the images through radio-frequency transmitters and the sensor array those are fixed at different locations on the anterior abdominal wall (Fig. 1.2) to the data logger, which is hanging on the patient. After the examination, the images are downloaded to a computer and investigated as

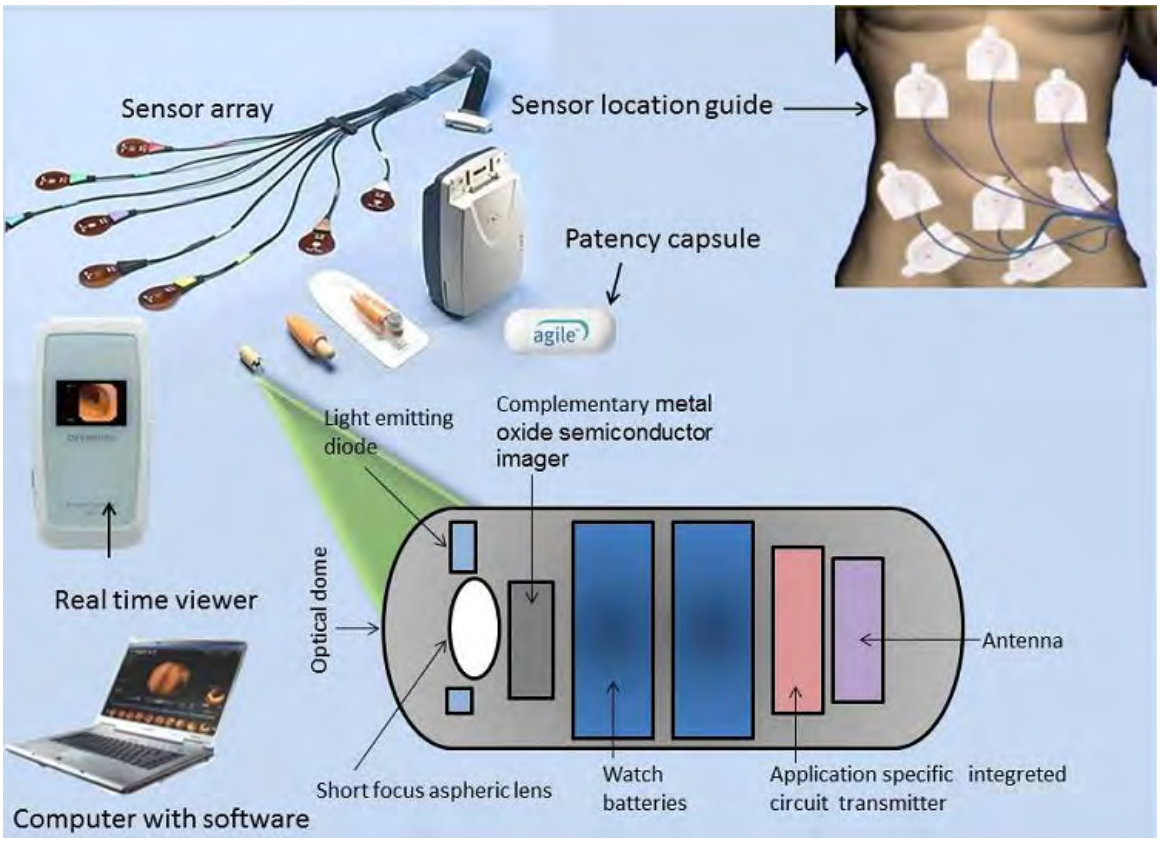

Fig. 1.2: Components of capsule endoscopy system including schematic representation of parts of capsule and sensor location guide; source: [1]

video images with software. The use of the real-time viewer may shorten procedures as the patient can be disconnected as soon as the suspected images are visualized [8]. Recently, software has been upgraded with additional capabilities to assist the reader, such as the ability to localize the capsule, blood indicator, a multi-viewing feature and quick view modality.

1.2.2 Bleeding Related Abnormalities in WCE

GI tract bleeding accounts for approximately 300,000 hospitalizations per year in the United States [9]. In the majority of the cases, the source of bleeding can be found with the traditional diagnostic methods. However, the source of bleeding cannot be readily identified in approximately 5% of patients [10]. These bleeding incidences with unknown origin are called obscure gastrointestinal bleeding (OGIB). The small bowel has been known to be one of the prime locations of lesions leading to OGIB. The visualization of the entire small intestine is not possible with upper endoscopy and colonoscopy. Technologies like WCE and push enteroscopy have recently been

Table 1.1: Specification of Capsule

	Pillcam SB2
Length (mm)	26
Weight (g)	3.4
Number of cameras	1
Frame rate per second	2
Image sensor	CMOS
Battery life (hr)	8
Number of Antenas	8

advanced to make the small intestine accessible for examination [11]. Also, among these two methods, it was studied that WCE is preferred by patients because of less pain and more ease and comfort associated with the procedure [12]. Other works have also shown that WCE has a larger range of access to the small intestine, and thus can identify more bleeding sites than push enteroscopy [12]. WCE has thus established itself as a gold standard tool in the examination of the small bowel.

1.3 Literature Review

Standard endoscopy and capsule endoscopy both have the ability to view the GI tract directly. However, the two systems have different operation scenarios. In standard endoscopy procedures, the diagnosis process is controlled by the physician. Given that the whole process is viewed by the physician in real time anyway; manual marking of suspicious regions is not time-consuming. But in the case of WCE, the pill-shaped device moves along the GI tract in a manner similar to food, which is through natural peristalsis. Thus, the diagnosis process is not controllable as the camera cannot be moved according to the desire of the endoscopist. The recorded video is then viewed later for examination. The real time viewing of the process is infeasible as the complete process lasts for an average of 8 hours. Also, the process produces around 55,000 frames per patient per examination and it requires around 2 hours of time for a physician to inspect the video [13]. Thus, there is a high scope of computer-assisted diagnosis tools in WCE for making the diagnosis more accurate, reliable and fast. The inspection time of the video can be greatly reduced if the suspicious frames could be recognized by a computer system. The suspicious frames

thus selected could then be presented to the physician for the final decision. Furthermore, there may be some bleeding regions and abnormal characters which cannot be recognized by naked eyes due to their size or distribution. All these problems motivate researchers to develop the computer aided intelligent bleeding detection technology in reducing the burden of physicians. Given Imaging (Yoqneam, Israel) provides a tool called Suspected Blood Indicator (SBI) that detects red pixel in the images [14]. However, studies have shown that performance of SBI is not sufficient to screen all types of bleeding in the GI tract [15], [16]. This has motivated a lot of studies in the development of computer-assisted diagnosis tools to automatically detect bleeding frames from WCE video and hence localize bleeding areas in a detected bleeding image.

A number of studies related to computer-aided diagnosis (CAD) in capsule endoscopy are pattern recognition problems that perform classification of images into different classes according to the image features. Image features characterize certain properties of images. Features that describe image properties, such as color, texture, brightness, contrast etc., have been widely studied and used in pattern recognition involving images. For the purpose of analysis, different color spaces are utilized, namely RGB (red-green-blue), HSV (hue-saturation-value), CMYK (cyan-magenta-yellow-black), YIQ, YUV, CIElab. The classification itself can be of various types based on the identification area, which is the area of the image that is used in the calculation of feature. It can range from whole image and image fragments to even the smallest image element i.e. the image pixel. The choice of an identification area for the mathematical formulation of the features depends on its appropriateness to the aim of the image analysis. According to the identification area, classification is performed in four ways: pixel-based, image-based, patch-based, and region-based.

Pixel-based methods analyze and classify every pixel in the images. Such a scheme are followed in [17], [18]. Both of these methods require multi-dimensional feature vector for processing every pixel in an image. In [17], both RGB and HSI color spaces are used to obtain features and for the purpose of classification probabilistic neural network (PNN) is considered. On the other hand, [18] uses artificial neural network (ANN) classifier. Classification based on this kind of feature extraction scheme requires a high computational cost for a single image, which gets

even worse for higher resolution images. As a result, these methods may require a long duration of time and may not be very effective for online WCE analysis. Also, features derived from a single pixel may not be a good representative of the local and global neighborhood.

Image-based methods ([19]- [20]) generate features utilizing the area of the whole image. The features thus characterize the whole images which are then subject to classification. In [19], [21], [22], image-based features like statistical feature obtained from the histogram, color plane histogram, and word based histogram are utilized. And for the purpose of classification probabilistic neural network (PNN) is used in [19] support vector machine (SVM) is employed in [21], in [22] both SVM and k-nearest neighbor (KNN) classifiers are used. In [20], Histogram variance control based bleeding detection scheme is proposed, where CIElab color space is applied to extract the features. The main advantages of image-based classification method are its simplicity and low computational cost in feature extraction and classification. However, delineation of the bleeding areas in the WCE image may not be possible directly from the extracted image-based features. While identifying the bleeding zones in a WCE image leads to another classification task, where a pixel-based classification may be suitable.

An intermediate area of identification is thus generally preferred in capsule endoscopy images where features are generated from image patches. Image patches are derived by dividing an image into blocks of fixed shape and size. One such example is to divide an image into rectangular blocks of 8×8 pixels. These image patches characterize local image features and are computationally less rigorous than pixel based schemes. Authors in [23] performed a classification based on image patches by dividing images (256×256 pixel resolution) into rectangular blocks of 30×30 pixels and similarly, in [24] classification based on blocks of 10×10 pixel on images of 400×400 resolution is performed. In [24], a threshold based approach of statistical parameters of each block is proposed. In [23], chrominance moment computed in each block in HSI color space is utilized as the color texture feature. In addition, uniform local binary pattern (LBP) is used to extract texture representation model, which is applied to discriminate normal regions and bleeding regions in WCE images. Classification of bleeding regions using the multilayer perceptron neural network is

then carried out. The main drawback of patch or block based methods is that it cannot accurately delineate bleeding zones due to arbitrary shape and size of bleeding regions. Moreover, the bleeding detection performance and computational cost highly depend on block size. However, block/patch based feature extraction mitigates single pixel randomness problem which is considered a common phenomenon in WCE. This block based feature extraction method has significant potential to detect bleeding images from WCE videos.

In region-based methods, instead of dealing with the entire image, certain regions are chosen for further processing. Image regions are image partitions of arbitrary shape and size which are derived by dividing an image into several pixel groups, such that the individual groups contain pixels which are similar to each other with respect to some criteria. Lesions are generally of arbitrary shapes and sizes which make fixed sized rectangular or circular patches unsuitable to serve as effective ROIs. In [25], a region growing method of bleeding image detection is developed. It is shown that all the features used in the study performed better classification when the features were derived from the image regions. One drawback of this method is that the initial bleeding seed needs to be marked manually, thus, this method is not fully automated rather semi-automated. Another region-based method is developed in [26], where a super-pixel segmentation is proposed to reduce the computational complexity while maintaining high diagnostic accuracy. A feature vector of each super-pixel is extracted using the red ratio in RGB color space and fed into a support vector machine (SVM) for classification. In regions based methods, bleeding detection performance extremely depends on the quality of selected regions of interest (ROI) and sometimes finding the ROI itself may need complex and computational expensive algorithm. Hence, there is still demand to develop a scheme which utilizes the advantage of both block and region-based approaches to enhance feature quality and improve classification performance.

1.4 Motivation of This Research

The motivation of this research is to develop efficient automated computer-aided methods to detect bleeding frames in WCE video. Once a bleeding image is detected in a WCE video, automatic marking of the bleeding zone by the bleeding

detection software is very much supportive for the reviewer to diagnose the diseases. Thus, another motivation is to introduce a bleeding zones detection scheme with high accuracy and tracking bleeding frames of a WCE video. In order to detect bleeding frame, we investigate image-based, block-based and combination of block and region-based feature extraction methods. In the image-based method, we introduced composite color plane and various statistical features. Color histogram feature is proposed for block-based analysis. In order to use the advantages of both block-based and region-based method a combination of block and region-based method is proposed using unsupervised clustering scheme. Very limited research has been done to detect bleeding zones. Detection of the bleeding zone with high accuracy is a challenging task. Thus, in this thesis, bleeding zone detection algorithm is also developed to delineate bleeding regions with high accuracy. Most of the methods described in the literature are reported performance result considering bleeding and non-bleeding dataset collected discretely from a number of WCE videos. It is to be noted that in test cases of CAD system, input data is a video file, thus, performance needs to be analyzed in continuous frames of a given video. However, the very limited paper reported video level performance. A fast-tracking of bleeding frames in WCE video is a difficult task. In this thesis, video level performance of different video clips is investigated and hence a post-processing algorithm is proposed using labeling decision of continuous frame.

1.5 Objectives and Scope

The objectives and Scope of this thesis are:

1. To propose efficient feature extraction schemes utilizing composite color plane and color histogram in WCE images.

2. To develop region-based feature quality enhancement scheme.

3. To develop post-processing scheme to obtain better accuracy in tracking video frames and verify the detection performance on continuous WCE videos

4. To identify bleeding region precisely in a detected bleeding frame

The outcome of this thesis is an automatic computer aided technique to detect bleeding frame and zone from WCE video recordings, which will help the physicians to diagnose different gastrointestinal diseases. However, detection of other abnormalities (like tumor, ulcer, polyp etc.), development of WCE device are beyond the scope of this thesis.

1.6 Organization of the Thesis

The rest of the thesis is organized as follows

In Chapter 2, a feature extraction is proposed utilizing the whole image (called holistic approach) in composite color space. A G/R composite plane is introduced. Different statistical features are investigated. A post-processing scheme is introduced that enhances the performance of bleeding frame detection in the continuous video frame. Finally, a bleeding zone segmentation method is proposed. Detail experimental results on the publicly available database are reported along with comparative performance analysis.

In Chapter 3, region-based feature quality enhancement method is proposed to detect bleeding frame. Here, at first, the given image is segmented into two clusters using local feature extracted from each block. Next, a global feature extraction method is introduced where cluster-specific features are used along with the differential cluster feature. Finally, the bleeding zone is detected from a bleeding image. Detail experimental results are presented considering a variation of block size and amount overlapped between consecutive blocks. Comparative performance analysis is also presented between proposed method and few recent papers from the literature.

In Chapter 4, a proposed color histogram based feature extraction method is presented. Instead of using intensity information of a single color plane, all three color planes are utilized in extracting color histogram feature, which is considered more prominent and consistent representation of bleeding. A feature reduction scheme is developed that reduces feature vector dimension. Performance result of color histogram feature is reported considering the block-based and cluster-based approach.

Chapter 5 summarizes the outcome of this thesis with some concluding remarks and possible future works.

Chapter 2

Pixel Based Feature Extraction of WCE Image

In this chapter, pixel based holistic feature extraction scheme is proposed for bleeding frame detection of WCE recordings. Unlike conventional methods, instead of directly using RGB color space, a transform color domain is introduced. Higher and lower order statistical analysis in transform color domain are carried out to extract feature from an entire image. Feature-based supervised classification using support vector machine (SVM) is performed to differentiate bleeding and non-bleeding images. Next, to improve the bleeding frame detection performance in WCE video, a post-processing scheme is developed using a variation of temporal characteristics of consecutive frames. Finally, a zone detection algorithm is proposed to identify bleeding regions in the detected bleeding images. Extensive experimentation is carried out on a numerous number of WCE images and videos. It is observed that the proposed algorithm can detect bleeding frame and bleeding zone from WCE video recordings with a satisfactory level of performance.

2.1 Bleeding Frame Detection

In this method, the feature is extracted considering the whole image (holistic approach). Workflow of the proposed method is illustrated in Fig. 2.1. The input of the proposed method is a WCE video segment, followed by preprocessing, domain transformation, feature extraction, classification and post-processing. The output is the label of the frames (bleeding or non-bleeding) and detected bleeding zone of a bleeding image. The WCE video recordings possess low frame rate, e.g. 2 frames/sec and generally the dimension of the image frame is 576×576. A circular region in the

given WCE image contains necessary information due to its constructional nature of intestinal pathway. Typical bleeding and non-bleeding WCE images are presented in Fig. 2.4. Figs 2.4 (a) and (b) presents bleeding images where red zone indicate bleeding. Note that in Fig. 2.4 (a) the presence of bleeding zone is very prominent while in the case of fig. 2.4 (b), it is very difficult to precisely locate bleeding zones. In Fig. 2.4 (c) and (d), non-bleeding images are shown, where red bleeding zones are absent. However, it is observed that in Fig. 2.4 (d) light red bleeding like areas appear which leads to confusion. Hence, just by looking at WCE images it may not always possible to differentiate bleeding and non-bleeding images. Moreover, automatic bleeding zone detection is also very difficult.

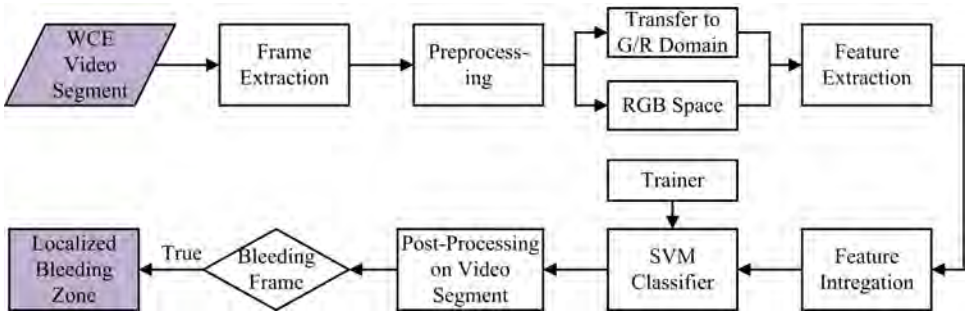

Fig. 2.1: Illustration of work flow of proposed method

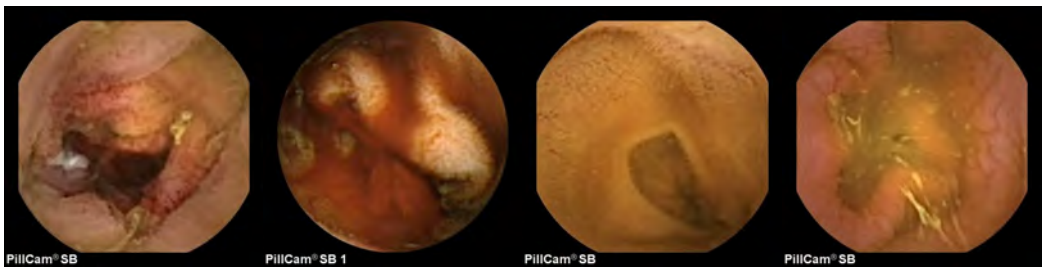

(a) (b) (c) (d)

Fig. 2.2: Examples of RGB WCE images. (a), (b) bleeding images, (c), (d) non-bleeding images

2.1.1 Preprocessing

In WCE video, images are captured at a regular interval and in each image, as mention before the necessary information is preserved in the central region (circular or semi-octagonal) as shown in Fig. 2.3 (a). Around the central zone of each image, there exist black regions carrying no information related to bleeding or non-bleeding

tissues. If the entire image is considered for feature extraction, the presence of these black surround pixels can degrade the quality of extracted features. It is observed that the pixels residing in the black outer zones possess extremely low-intensity value with respect to the pixels of the desired central zones. In the proposed method, at the beginning, black pixels of the outer zone are removed considering the change in pixel values and circular shape of the desired region. Fig. 2.3 represents the step by step output during removing the undesired outer black zones. First, the black portions of the four sides (left, right, top, and bottom) are removed, which is demonstrated in Fig. 2.3 (b) and then the black portions located in the corner areas are removed. The extracted image contains the required information and demonstrates characterization and description of WCE. Instead of using the entire image, the resulting black-boundary pixel eliminated images are considered for further processing, which makes feature extraction procedure much effective and involves less computational burden.

(a) (b) (c)

Fig. 2.3: Illustration of preprocessing step: (a) original WCE frame; (b) after removing black portions of the four sides; (c) final preprocessed image after removing corner black regions.

2.1.2 Transformation from RGB to a Composite Plane

Various color spaces are used by different researchers to visualize bleeding regions in WCE images [22], [25], [27]. Among them, RGB color space is most widely used for detecting bleeding images in WCE video. The reasons behind such a practice are: (i) the available format of WCE images use RGB color space and (ii) there is a common understanding that the color of bleeding belongs to specific shades of red. Because of intensity level variations of R, G, and B, different shades of a particular color can be obtained. For example, red $(255, 0, 0)$, maroon $(128, 0, 0)$, dark red $(139, 0, 0)$ and firebrick $(174, 34, 34)$ have different RGB values (which are provided

inside the parenthesis). Bleeding zones in a WCE image may contain different shades of red and also the non-bleeding images may contain similar shades. Hence, it is very difficult to identify bleeding zones directly from the RGB intensity values. Another important factor affecting the bleeding zone detection in WCE images is the change in illumination during the long duration of the endoscopy. One possible reason behind the illumination variation is capsule's battery weakening over time. It is found that the change in illumination causes intensity variation in R, G, and B planes intensively. This unwanted intensity variation may hinder usual intensity pattern due to the presence of bleeding and non-bleeding zones. As a result, it will play a detrimental role in feature extraction.

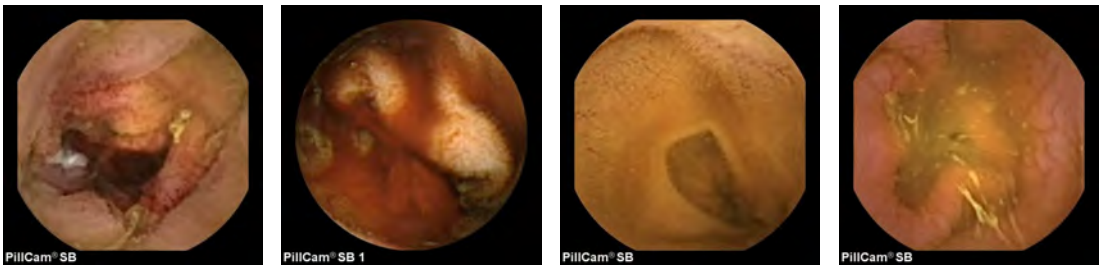

(a) (b) (c) (d)

Fig. 2.4: Examples of RGB WCE images. (a), (b) bleeding images, (c), (d) non-bleeding images

In Fig. 2.4, examples of WCE images (bleeding and non-bleeding) in RGB color plane are shown. It is observed that in the case of bleeding images size and shape of bleeding zones vary significantly. In Fig. 2.4(a) a small portion is bleeding and in Fig. 2.4(b) comparatively larger portion is bleeding. In the case of non-bleeding images, bleeding like zones may appear as shown in Fig. 2.4(d). In order to demonstrate the variation in intensity distribution between bleeding and non-bleeding zones, in Fig. 2.5, histograms of intensity levels of red, green and blue planes are shown considering two bleeding and non-bleeding images presented in Fig. 2.4. From the figure, it is observed that intensity distribution in bleeding zones shows interesting characteristics, almost no overlaps between R and G planes and R and B planes. However, in non-bleeding zones, severe overlaps are observed in the combination of any two RGB planes. This gives an idea that instead of dealing with a single plane, a combination of two planes may provide more discriminating characteristics. In order to further understand the tendency of pixel values, two-

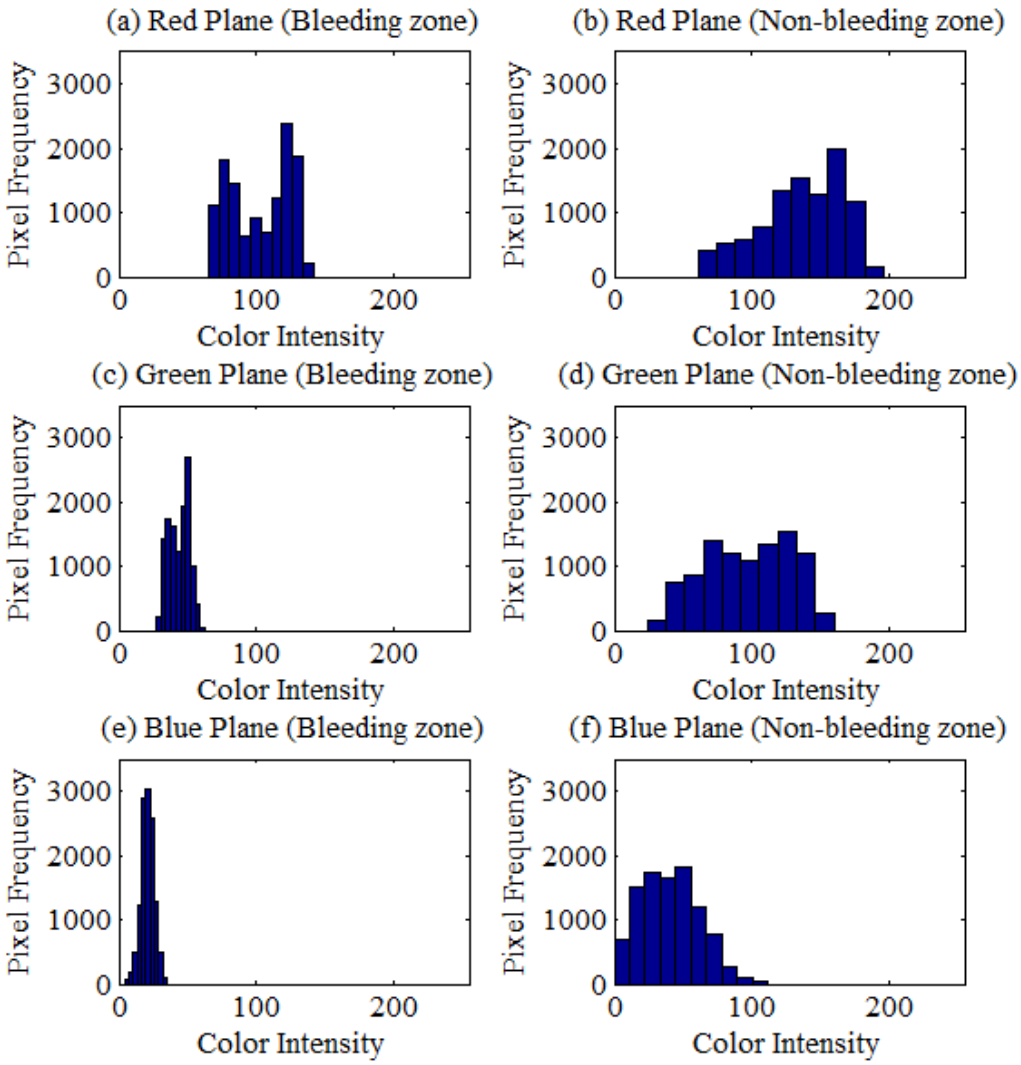

Fig. 2.5: Histogram obtained from bleeding and non-bleeding zones in different color planes: (a) red plane of bleeding zone; (b) red plane of non-bleeding zone;(c) green plane of bleeding zone; (d) green plane of non-bleeding zone; (e) blue plane of bleeding zone; (f) blue plane of non-bleeding zone

dimensional plots considering G-R and B-R planes are shown in Fig. 2.6. Since a large amount of overlaps exists between G and B planes, G-B combination is ignored. It is to be mentioned that in literature it is well established that the intensity distribution in the blue plane does not carry significant information in discriminating bleeding and non-bleeding zones [28]. From Fig. 2.6(b) it is found that in B-R plot, bleeding and non-bleeding pixels are largely overlapped. On the other hand, it is clearly observed in Fig. 2.6(a) that G-R plot offers separability of bleeding and non-bleeding pixels. In this case, pixels with high G values and low R values and vice versa. From R-plane and G-plane histograms, one can easily

notice that R values are relatively higher in this figure approximately higher than 70 and G values are lower (approximately less than 70). As a result, considering a composite plane consisting of the ratio of intensity values of G and R planes can provide a better option for bleeding pixel detection in comparison to using a single (G or R) plane. The ratio plane is expected to offer narrow band histogram and help in reducing the effect of unwanted pixel intensity variation due to illumination change.

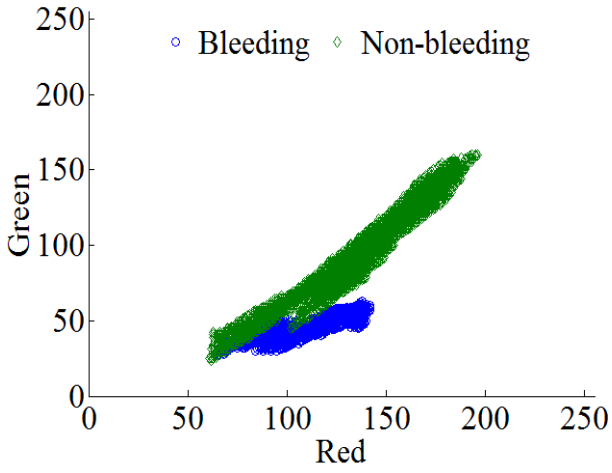

(a)

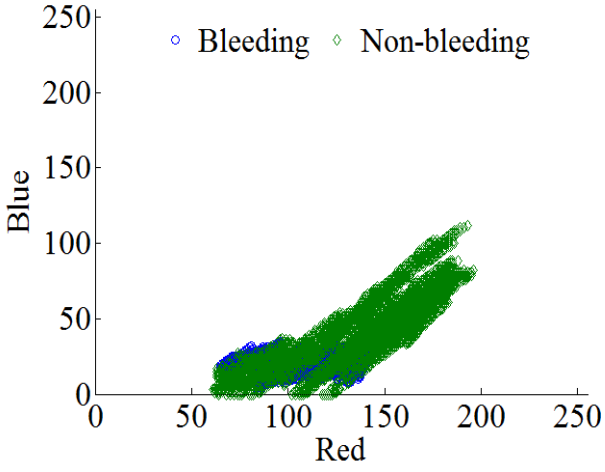

(b)

Fig. 2.6: Bleeding and non-bleeding pixel distribution, (a) distribution in RG in 2D space, (b) distribution in RB in 2D space

In order to investigate the histogram characteristics of composite planes constructed from the ratios of intensity levels, different combinations of red, green and blue planes are considered. In Fig. 2.7, histograms of bleeding and non-bleeding

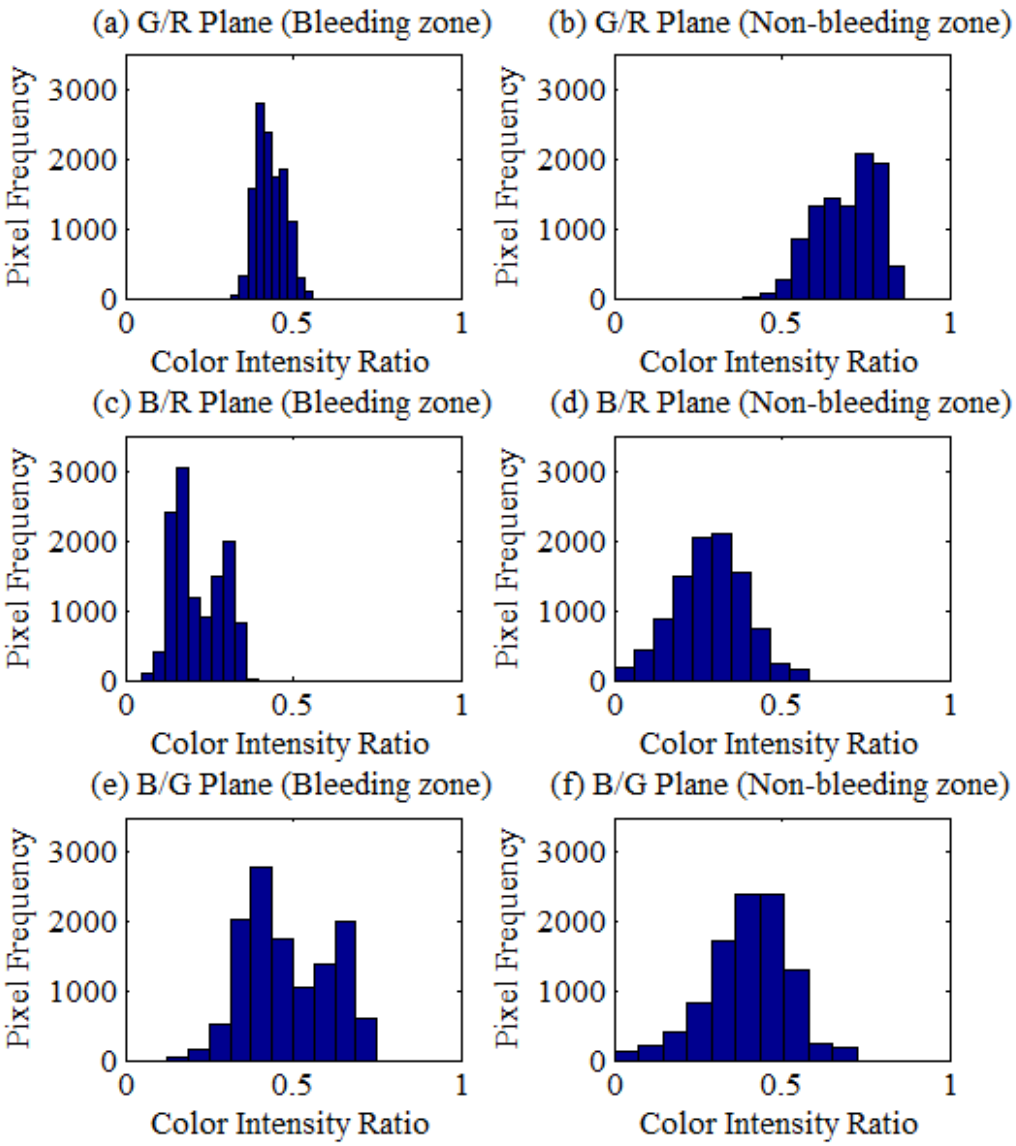

Fig. 2.7: Histogram obtained from bleeding and non-bleeding zones in different ratio planes: (a) green to red ratio (G/R) plane of bleeding zone; (b) green to red ratio (G/R) plane of non-bleeding zone; (c) blue to red ratio (B/R) plane of bleeding zone; (d) blue to red ratio (B/R) plane of non-bleeding zone; (e) blue to green ratio (B/G) plane of bleeding zone; (f) blue to green ratio (B/G) plane of non-bleeding zone.

zones in different ratio planes are shown. In Figs. 2.7 (a) and (b), green to red (G/R) transformed domain is considered. It is observed that a narrow band histogram is obtained in comparison to those shown in Fig. 2.5. Moreover, it exhibits quite separable histogram patterns between bleeding and non-bleeding cases with the reasonably small amount of overlap. Similarly, in Figs. 2.7 (c)-(f), histograms considering blue to red (B/R) transformed domain and blue to green (B/G) transformed domain are shown. As it is already mentioned that the blue plane does

not carry significant information to distinguish between bleeding and non-bleeding zones, the histograms shown in Figs. 2.7 (c)-(f) do not exhibit narrow band pattern and contain a significant amount of overlaps. Hence in the proposed method, we propose to use a composite plane constructed from the pixel intensity ratio of green and red planes, namely G/R pixel ratio plane. Feature extraction is carried out from G/R plane, which is expected to overcome the problems of unwanted illumination variation and inconsistencies in intensity pattern in various bleeding zones.

2.1.3 Statistical Feature Extraction from G/R Domain

Statistical features are acquired from images and tested successively to find the best-suited combination of features to be used for detecting bleeding images. Apart from most commonly used first and second order Statistical measures, e.g. mean, median, mode, variance, maxima, and minima, some higher order measures are also utilized e.g. kurtosis, and skewness. In what follows, the necessary formulas used for calculating the above statistical parameters are presented

Mean: The mean is the arithmetic average of a set of values. In the images, mean is defined as summation of pixel intensities divided by total number of pixels. If the presented regions in WCE image contain N_T pixels and an i-th pixel located at (x_i, y_i) has pixel intensity ratio $C(x_i, y_i)$ then mean is calculated as

$$\mu = \frac{1}{N_T} \sum_{i=1}^{N_T} C(x_i, y_i); \quad N_T = total\, no.\, of\, pixels \tag{2.1}$$

Mode: The mode is the value that appears most often in a set of data i.e., which is most frequent. In G to R intensity ratio plane WCE image, the mode is defined as the ratio which occurs most.

Variance: Variance is a measure of dispersion. It is the average squared distance between the mean and each item in the population or in the sample. Mathematically for WCE images

$$\sigma^2 = \frac{1}{N_T} \sum_{i=1}^{N_T} \big(C(x_i, y_i) - \mu\big)^2 \tag{2.2}$$

where μ is the mean defined in equation 2.1 and $C(x, y)$ is the G to R pixel intensity ratio.

Median: The median is the numerical value separating the higher half of a data sample or a population from the lower half. The median of a finite list of numbers

can be found by arranging all the observations from the lowest value to the highest value and picking the middle one. In WCE images, median is calculated from the pixel intensity ratio plane.

Kurtosis: Kurtosis characterizes the relative peakedness or flatness of a distribution compared with the normal distribution. It is define as

$$Kurtosis = \frac{M_4}{\sigma^4} \tag{2.3}$$

where M_4 is the fourth moment about the mean k-th moment about the mean is defined as

$$M_4 = \frac{1}{N_T} \sum_{i=1}^{N_T} \big(C(x_i, y_i) - \mu\big)^k \tag{2.4}$$

where μ is the mean defined in equation 2.1 and $C(x, y)$ is the G to R pixel intensity ratio.

Skewness: Skewness is the measure of asymmetry of a data set or distribution about its mean. The skewness value can be positive or negative, or even undefined. Mathematically it is the ratio of the third moment (M_3) and the second moment ($M_2 = \sigma^2$) which is raised to the power of 3/2 and defined as

$$Skewness = \frac{M_3}{M_2^{3/2}} = \frac{M_3}{\sigma^3} \tag{2.5}$$

Maxima and Minima: The largest value of a data set is known as maxima while the smallest value is called minima.

Using above definitions, the statistical parameters are calculated in G/R pixel intensity ratio domain and used as features for bleeding detection. The behavior of each statistical parameter for bleeding and non-bleeding images is investigated.

Proposed Pixel Intensity Ratio Count Feature

It is well known that red is the most dominating color that naturally helps in identifying bleeding. Hence, while considering the intensity ratio planes in RGB color space, the level of pixel intensity values of other two colors (G, B) with respect to red (R) pixel intensity may help in extracting bleeding characteristics. However, from the sample distribution is shown in Fig. 2.7, only G to R ratio plane exhibits capabilities of distinguishing characteristics between bleeding and non-bleeding pixel. In this case, it is observed that the distributions of bleeding and non-bleeding pixels are

clearly separable. Thus, a threshold value of G/R pixel ratio ($T_{G/R}$ can be chosen to differentiate pixels into two classes. It is expected that bleeding zone pixels will have G/R pixel intensity ratio less than $T_{G/R}$ and non- bleeding zone pixels possess ratio value greater than $T_{G/R}$. From these observations, in the proposed method, the number of pixels in an image that satisfies condition i.e., $C(x_i, y_i) \leq T_{G/R}$ is counted. The threshold value can be obtained based on histogram presented in Fig. 2.7 and experimental result using several bleeding and non-bleeding images. This pixel intensity ratio count is also used as a feature in the proposed method. 2.8, the distribution of pixel intensity ratio count feature is presented in box plot for 400 WCE images (200 bleeding images and 200 non-bleeding images). In the figure, left and right side box represents the feature acquired from bleeding and non-bleeding images respectively. For the purpose of acquiring box plot, the value of $T_{G/R}$ is set as $\frac{1}{2}$. From the box plot, it is found that feature from non-bleeding images concentrated in a very small range with very low centroid value. However, for bleeding images, it is found that ratio-count feature distributed in a wide range, it exhibits well-separated centroid value from the non-bleeding image. It is also shown that intensity ratio feature has non-overlapping (marginally overlapped) characteristic thus it can be referred, this feature is highly separable for bleeding detection in WCE images.

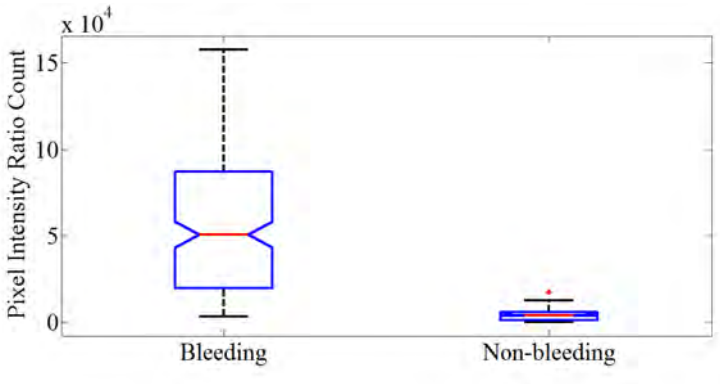

Fig. 2.8: Color ratio distribution of WCE images.

Average Intensity in Different Color Planes

Color texture statistical feature in terms of average pixel intensity of R, G, and B color planes is also incorporated in the overall feature vector in order to enhance the feature quality. The mean pixel intensity E_i of j-th color plane can be calculated

using the following equation

$$E_j = \frac{1}{N_T} \sum_{i=1}^{N_T} I_j(x_i, y_i) \tag{2.6}$$

Hence, apart from statistical features, pixel intensity ratio count and three mean intensities of R, G, B are included in the proposed feature vector.

2.1.4 Classifier

K-nearest Neighbor (KNN) Classifier

To classify the bleeding and non-bleeding WCE images the K-nearest neighbor (KNN) classifier is used. Because of its simplicity and satisfactory performance, KNN is one of the most widely used classifiers in several pattern recognition problems. It classifies the test WCE image by comparing the extracted feature with K neighboring feature obtained from train data set by considering a distance function. After classification, the KNN classifier provides a class membership. This class membership assigned to a test object is determined from votes of the majority K nearest neighbors. In the proposed method, Euclidean distance is used to classify test image considering the class labels of K nearest image patterns. Different values of K can be used and thus, the classification performance is tested by varying K values. However, if the quality of extracted features is good, less variation in classification performance will be observed with respect to different K values.

Support Vector Machine (SVM) Classifier

In the proposed method, the support vector machine (SVM) is also employed to classify the test WCE images. The key component in SVM learning is to identify a set of representative training vectors deemed to be the most useful for shaping the (linear or nonlinear) decision boundary. These training vectors are called support vectors, which need to lie right on the marginal hyper-planes.

Considering a training dataset which consists of expression profiles of N images x_i, where each M dimensional expression profile $x_i = x_i(n), n = 1, \cdots, M$ is associated with a teacher value or class label (e.g. bleeding and non-bleeding). Given a discriminant function $f(x) = f(w, x)$, the objective is to find an M dimensional decision vector $w = [w_1\ w_2\ \cdots\ w_M]^T$ so that $f(x_i)$ can best match with teacher

value y_i, with all the training dataset taken into consideration. Considering 2 class problem with teacher values $+1$ and -1, in the basic SVM, all the training vectors x_i satisfy the following inequalities:

$$w^T x_i + b \geq +1, \ \textit{for all positive } x_i$$

$$w^T x_i + b \leq -1, \ \textit{for all negative } x_i \tag{2.7}$$

An error term is defined as $\epsilon_i \equiv w^T x_i + b - y_i$. The main objective here is to create a maximum margin to separate the two opposite classes. Maximization of the separation margin $2/\|w\|$ can be achieved by minimizing $\|w\|$. Apart from this, considering a set of slack variables $\{\xi_i\}_{i=1}^N \geq 0$, the optimization formula can be written as

$$min_w = \Big\{\frac{1}{2}\|w\|^2 + C\sum_i \xi_i\Big\}, \ \textit{subject to } y_i\epsilon_i + \xi_i \geq 0 \tag{2.8}$$

The above quadratic programming optimization problem is solvable by using convex optimization techniques, more specifically, by using a Lagrangian one can obtain the following Wolfe dual-optimization formulation in terms of empirical vector $\mathbf{a}$

$$max_a \ L(\mathbf{a}) = \mathbf{a}^T y - \frac{1}{2}\mathbf{a}^T\mathbf{K}\mathbf{a} \tag{2.9}$$

subject to

$$\sum_{i=1}^N a_i = 0, \ \mathbf{w} = \sum_{i=1}^N a_i \mathbf{x}_i, \ 0 \leq a_i y_i \leq C, \ i = 1, \cdots, N$$

where kernel matric $\mathbf{K}$ is given by

$$\mathbf{K} = \begin{bmatrix} K(x_1, x_1) & K(x_1, x_2) & ... & K(x_1, x_N) \\ K(x_2, x_1) & K(x_2, x_2) & ... & K(x_2, x_N) \\ \vdots & \vdots & ... & \vdots \\ K(x_N, x_1) & K(x_N, x_2) & ... & K(x_N, x_N) \end{bmatrix} \tag{2.10}$$

and it is jointly determined by the kernel function $K(x, y)$ and the training vectors. After $\mathbf{a}$ is learned, the decision boundary is characterized by $f(x) = 0$, where $f(x)$ is the discriminant function defined as

$$f(x) = \sum_{i=1}^N a_i K(x_i, x) + b \tag{2.11}$$

It is to be mentioned that the (i, j)-th element of the kernel matrix can be defined as the inner product of the i-th and j-th training vectors. A nonlinear kernel function

can also be adopted as the inner product. In the proposed scheme, most widely used radial basis function (RBF) is used as the kernel, which is an exponential function. It is shown that the kernel approach hinges upon the mapping from the original space to a new representative vector space. Moreover, the number of basis function for the kernel vector space is usually (much) greater than the dimension of the original feature space. This plays a major role facilitating the design of highly discriminant classifiers. This is the major reason why the kernel based approach is usually much more effective for supervised classification.

2.1.5 Post-Processing

In previous subsections, a complete method of classifying a test WCE image as bleeding or non-bleeding is proposed. In the WCE based diagnosis, generally, the objective is to find out the bleeding frames in a WCE video recording. In this case, each frame of a given WCE video needs to be tested. However, in most of the reported literature, for the performance evaluation, instead of using the entire WCE video, a set of bleeding and non-bleeding images collected from different WCE video recordings are used [22], [27], [23]. In the result section, the bleeding detection performance of the proposed method using such a set of bleeding and non-bleeding images is also presented. Apart from this, considering that the video recording or the sequential WCE frames are available, in this subsection, a post-processing algorithm is proposed where prior to finalizing the decision on a test image, preliminary decisions on neighborhood frames are taken into consideration. Depending on the preliminary decisions of nearby frames of a test image, the decision of that test image is either preserved or revised. Based on extensive experimentation on several bleeding and non-bleeding video recordings, it is found that in general, an isolated bleeding or non-bleeding frame does not appear, rather similar types of frames appear in consecutive frames. Even similar type of frames (either bleeding or non-bleeding), appearing less than three consecutive frames is rarely observed. In the proposed post-processing scheme, instead of dealing with entire video at a time, consecutive small portions of videos, each consisting of a certain number of frames (L) are sequentially tested. In order to test a frame, an equal number of prior and post frames in the neighborhood of that particular test frame are taken

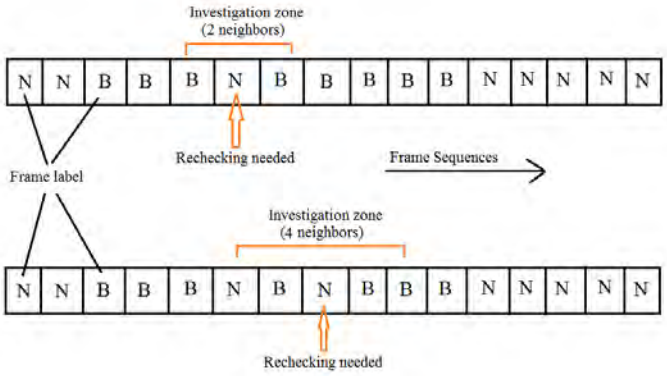

Fig. 2.9: Illustration of post processing scheme

into consideration. For example, for testing a frame which is preliminary declared as non-bleeding, if two post and prior frames are considered along with the test frame, there will be in total five frames under investigation. Based on the majority voting principle, when the majority of frames possess labels opposite to the label of the test frame, further checking is proposed to finalize the label of that test frame. In the example case stated before, for the non-bleeding (N) test frame, among four neighborhood frames under investigation, if three of them are labeled as bleeding (B), according to the proposed hypothesis, the test frame needs to be checked again. Thus, for a non-bleeding test frame, if one post and prior frames are considered (in total three frames), among possible four cases (NNN, NNB, BNN, BNB) only one case (BNB) needs to be rechecked. Similarly, if two post and prior frames are considered (in total five frames), among 2^4 cases (xxNxx, x may be N or B), five cases need to be rechecked. In general, considering in total r number of frames, among $2^{(r-1)}$ cases, total $\sum_{i=(r+1)/2}^{r-1} {}^{r-1}C_i$ cases need to be rechecked. With the implementation of the rechecking process, there is a possibility of changing the preliminary decision of a test image, which may not be a good idea especially for images having preliminary bleeding labels. The reason behind of that, changing mistakenly the label of a bleeding image may have severe consequences in comparison to the case where a non-bleeding image is mistakenly labeled as bleeding. As a result in the proposed method of post-processing, only images having preliminary non-bleeding labels are considered. For better visualization, the proposed post-processing scheme is pictorially illustrated in Fig. 2.9. In the figure, test image and its corresponding investigation zone are presented with the help of frame sequences.

For the purpose of rechecking a distance based criteria using proposed feature vector is proposed. As described before, from each image features are extracted. Bleeding labeled image corresponds to bleeding feature ($\mathbf{F}^b$) and similarly non-bleeding image corresponds to non-bleeding feature ($\mathbf{F}^n$). The objective is to investigate whether a true bleeding image is incorrectly labeled as non-bleeding image or not. It is sufficient to compute two types of feature distances, 1) feature distance between bleeding and test frame ($\mathbf{d}^b$) and 2) feature distance between non-bleeding and test frame ($\mathbf{d}^n$). Therefore, the feature distance form bleeding feature (D^b) and non-bleeding feature (D^n) are calculated as following

$$\mathbf{d}_i^b = |\mathbf{F}_i^b - \mathbf{F}^t| \tag{2.12}$$

$$D^b = \frac{1}{P}\sum_{i=1}^{P} \mathbf{d}_i^b \tag{2.13}$$

$$\mathbf{d}_i^n = |\mathbf{F}_i^n - \mathbf{F}^t| \tag{2.14}$$

$$D^n = \frac{1}{Q}\sum_{i=1}^{Q} \mathbf{d}_i^n \tag{2.15}$$

where, $\mathbf{F}^t$ = feature vector of test frame

$\mathbf{F}_i^b$ = feature vector of i-th bleeding label frame

$\mathbf{F}_i^n$ = feature vector of i-th non-bleeding label frame

$\mathbf{d}_i^b$ = distance feature vector between an i-th bleeding label image and test frame

$\mathbf{d}_i^n$ = distance feature vector between an i-th non-bleeding label image and test frame

P = total number of bleeding label images in an investigation pool

Q = total number of non-bleeding label images in an investigation pool

To take the final decision, whether the label of test frame needs to be changed or not, following conditions are tested.

- if $D^b > D^n$, mark test frame as non-bleeding

- if $D^b < D^n$, mark test frame as bleeding
- if $D^b = D^n$, previous decision is kept

In this process, according to the condition of feature distance previously declared non-bleeding frame may be revised to bleeding.

2.2 Bleeding Zone Detection

Once a bleeding image is detected in a WCE video, it would be helpful for the user if bleeding zones in that image can be automatically marked. Automatic bleeding zone detection can provide several advantages, namely

- Quick visualization of the region of interest intensively
- Finalizing the bleeding detection decision of that image
- Further detail analysis on that bleeding region
- Investigating the change in bleeding characteristics in consecutive video frames.

Most of the available bleeding detection methods do not offer automatic bleeding zone detection facility. However in this research, an automatic bleeding zone detection scheme is proposed, which is applied for identifying bleeding regions in detected bleeding frames. To detect bleeding pixel, a threshold based method in G/R pixel intensity domain is proposed. At first, an edge detection algorithm is implemented to sort out the edges. Then, a threshold value is imposed to label bleeding pixel and finally Fine tune of bleeding zone with the help of morphology operation. Major steps, to be performed in the proposed bleeding zone detection algorithm are given below

- Detect edge and remove it from the given image
- Impose threshold to detect bleeding pixels
- Fine tuning of bleeding zone with the help of morphology operation.

The objective of this section is to detect bleeding zone from a bleeding WCE image. Generally, it is observed that edge of the WCE image does not contain

any bleeding pixels. Thus, from the common understanding, the edge regions of a bleeding image should be detected and removed. For the purpose of edge detection "Sobel method" is implemented [29]. This method finds edges using the Sobel approximation to the derivative. It returns edges at those points where the gradient of pixel intensity is maximum. After detecting the edges of a given image, it is removed from the image.

In order to detect bleeding pixels in the bleeding image, simple threshold-based method is introduced. As observed in Fig. 2.7, bleeding pixels are concentrated below the threshold value ($T_{G/R}$) of $\frac{1}{2}$ and on the other hand non-bleeding pixels are concentrated above that threshold value. Thus, in G/R domain, to detect bleeding zone, the $T_{G/R}$ value is considered around $\frac{1}{2}$, below that threshold value all the pixels are marked as bleeding pixels. To find out the effective $T_{G/R}$ value, a quantitative analysis is performed by varying the value of $T_{G/R}$ considering both positive and negative increment (small amount e.g. 0.05) around $\frac{1}{2}$ to archive the best performance result, which is reported in result section.

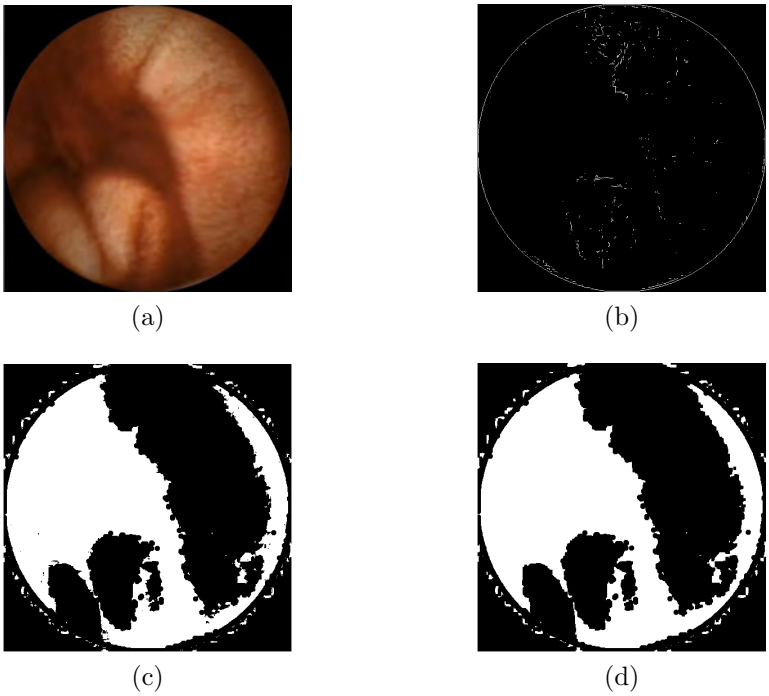

Fig. 2.10: Illustration of bleeding zone detection steps, (a) bleeding image, (b) edge regions, (c) after applying threshold, (d) output of morphological operation

2.2.1 Fine Tuning of Bleeding Zone Using Morphology Operation

Threshold-based operation provides a set of suspected bleeding pixels in the bleeding image. Generally, a single isolated pixel may not be a candidate for the bleeding zone. Such pixels may arise due to intensity variation or the presence of bleeding like areas. Choice of the hard threshold is also a reason for the appearance of isolated bleeding pixels. Discarding such isolated bleeding suspected pixels is not a good solution. Alternately we proposed to check the homogeneity around that suspected pixel. In this regard, morphological operations are performed, a namely morphological dilation followed by morphological erosion.

Morphological dilation offers connectivity among closely separate bleeding regions in a WCE image. It includes very small isolated non-bleeding regions or pixels if those are surrounded by bleeding regions. Apart from that it also dilates the boundary of bleeding regions. This operation ensures not to lose any bleeding pixels that are initially marked as bleeding rather than it enhances bleeding (foreground) regions with respect to non-bleeding (background). After Morphological dilation, morphological erosion operation is performed. Morphological erosion discards isolated regions (very small) and pixels those are a candidate for bleeding zones. It also erodes and smoothen the boundary of the bleeding zone. Hence, erosion operation ensures that bleeding zone must contains significantly large bleeding areas. Illustration of bleeding zone detection steps is presented in Fig. 2.10. In Fig. 2.10 (a) a bleeding image is displayed. Bleeding zone of that image is desired to identify. After applying edge detection algorithm, the edge of that bleeding image is acquired and displayed in Fig. 2.10 (b). Then, from the bleeding image, edges are subtracted. After that, threshold based method is deployed upon subtracted images and the output is represented in Fig. 2.10 (c). Finally, morphology operation is performed to obtained final bleeding zone, which is shown in Fig. 2.10 (d). Bleeding zone detection performance analysis are presented in the result section.

2.3 Results and Analysis

2.3.1 Bleeding Frame Detection Criteria

There are four cases about the detection result of bleeding and non-bleeding images. Namely: 1) true bleeding (T_b), 2) true non-bleeding (T_{nb}), 3) false non-bleeding (F_{nb}) and 4) false bleeding (F_b). There are two possible cases of false detection, 1) when a bleeding image is wrongly detected as a non-bleeding image (F_{nb}) and 2) when a non-bleeding image is wrongly detected as bleeding image (F_b). In a similar way, there are two possible cases of true detection, 1) when a bleeding image is correctly detected as bleeding image (T_b) and 2) when a non-bleeding image is correctly detected as a non-bleeding image (T_{nb}). To assess the capability of the bleeding detection method, accuracy, sensitivity and specificity [30] are ideal criteria, which are calculated as follows.

$$Sensitivity = \frac{\sum T_b}{\sum T_b + \sum F_{nb}} \tag{2.16}$$

$$Specificity = \frac{\sum T_{nb}}{\sum T_{nb} + \sum F_b} \tag{2.17}$$

$$Accuracy = \frac{\sum T_b + \sum T_{nb}}{\sum T_b + \sum F_{nb} + \sum T_{nb} + \sum F_b} \tag{2.18}$$

Sensitivity is a measure of correctness in bleeding frame detection. Specificity indicates truthfulness in identifying non-bleeding images. Accuracy reflects overall correctness of true bleeding and non-bleeding frame detection. For all these performance indicators, higher the values better the performance. For bleeding frame detection, sensitivity plays the most vital role because it is directly associated with the true bleeding frame detection truthfulness and always being the prime concern in bleeding frame detection research.

2.3.2 Data Acquisition and Experimental Setup

Extensive simulations are performed in order to demonstrate the effectiveness of the proposed method for bleeding frame and zone detection. For the purpose of simulation, several WCE videos are collected from a publicly available widely used database [31]. The database provides the ground truth labeling of bleeding and non-bleeding videos. The experimentation is carried out on those WCE videos and the results are reported on 20 of them, where 10 videos are labeled as bleeding and

10 are normal. Images in bleeding videos are manually annotated as bleeding or non-bleeding and if bleeding, the bleeding zones are marked by expert physicians. Bleeding frame detection results are reported for 2350 WCE frames, where 450 are bleeding and 1900 are non-bleeding, which are extracted from those videos. The performance of the proposed method in terms of bleeding detection criteria is investigated and compared with that of some of the recent methods. In what follow, first, the performance of bleeding frame detection is presented considering the effect of various parameters. Next, the bleeding detection performance in continuous WCE video clip is reported considering the effect of post processing. Finally, the bleeding zone detection performance is reported considering some bleeding images.

2.3.3 Performance of Bleeding Image Detection

At first, In Table 2.1, the accuracy of bleeding detection obtained by using different combinations of statistical features is presented. For the purpose of classification SVM classier with linear kernel is used. It is found that among different combinations of statistical features, a combination of median, variance and kurtosis exhibits the best accuracy of 94.97%. Thus, from G/R domain, median, variance and kurtosis are considered as proposed feature and named as statistical feature from G/R domain (Stat (G/R))

Table 2.1: Performance Comparison among Different Feature Combination in G/R Domain

Features	**Accuracy**
median, mean, mode	91.50%
median, variance, kurtosis	94.97%
mean, variance, kurtosis	90.50%
variance, mode, maxima	89.00%
mode, skew, kurtosis	88.50%
mean, skew, mode	90.00%
skew, mode, minima	89.50%
mean, skew, mode, maxima, minima	87.50%
mean, skew, maxima	84.50%
skew, mode, maxima	84.50%
mode, maxima, minima	84.00%
mean, skew, minima	83.50%

The performance of bleeding image detection of WCE video recording using

G/R ratio count and mean intensity of R, G, and B are presented below. By investigating several bleeding and non-bleeding WCE images available in [31], the threshold for pixel intensity ratio is kept as $T_{G/R} = 0.5$. In Table 2.2, performance variations of threshold values is presented. Here, PIR means pixel intensity ratio. It is observed that the performance is very satisfactory in the neighborhood of chosen threshold, which is also expected from Fig. 2.7. This feature is called pixel intensity ratio count (PIRC). Bleeding detection performance considering different features and their combination are reported in 2.3. From the table, best performance is obtained by the combination of PIRC, mean of red, green, blue and stat (G/R). The combination of this feature vector is called ratio count and statistic (RC & Stat) feature.

Table 2.2: Effect of Variation of Color Ratio on Performance Measures

Detection Criteria	**PIR** ≤ 0.4	**PIR** ≤ 0.5 **(proposed)**	**PIR** ≤ 0.6
Sensitivity	94.50%	94.78%	87.00%
Specificity	91.75%	93.58%	91.38%
Accuracy	92.30%	94.00%	90.50%

Table 2.3: Performance Comparison among Different Features

Feature	**Feat. Dim.**	**Sen.**	**Spec.**	**Accu.**
Stat (G/R)	3	91.37%	96.05%	94.97%
PIRC, mean (R, G, B)	4	94.32%	93.74%	93.83%
Stat (G/R), PIRC, mean (R, G, B)	7	97.75%	97.99%	97.96%

In Table 2.4, different performance measures obtained by the proposed method are presented considering three different types of classifier, namely K-nearest neighbor (KNN) SVM-linear, SVM Gaussian radial basis function (RBF). Among these three classifier, it is observed that the SVM linear kernel exhibits the highest sensitivity. Although highest specificity and accuracy is obtained by SVM-RBF classifier, SVM-linear classifier is proposed considering sensitivity and robustness nature of linear kernel.

For the purpose of comparison, the result obtained by the proposed method is compared with those obtained by the methods proposed in [23], [19], [32], [28], [27],

Table 2.4: Performance Measures Obtain by Different Classifier

Classifier	**Sensitivity**	**Specificity**	**Accuracy**
KNN (k=1)	83.54%	97.15%	94.51%
SVM linear	97.75%	97.99%	97.96%
SVM RBF	97.41%	98.66%	98.47%

[33], [34]. It is to be mentioned that the LBP features [23] are extracted independently from HSI color space. Here, uniform LBP acquired from plane I (intensity) of HSI color space and histogram values of uniform LBP are used as feature. In the implementation of the method proposed in [19], best feature combination, which are histogram probability, mean and energy of R, G, and B color plane are used. Intensity ratio and mean (R, G, B) features are presented in [32]. While statistical feature in R/G domain and Hue space are proposed in [28] and [33] respectively. ROI based feature extraction is presented in [27] and [34]. In [27], statistical feature from CMYK color space is proposed while in [34] statistical feature of Y.I/Q composite color domain is developed. For a fair comparison, in all the methods, experiments are carried on using the same classifier, i.e., SVM. The comparison results are demonstrated in Table 2.5. It is clearly observed that the proposed method exhibits the best performance in terms of all performance indices. Sensitivity is the most important performance index in bleeding detection, which represents the true bleeding image detection accuracy. It can easily be observed that the sensitivity obtained by the proposed method is extremely satisfactory.

Table 2.5: Comparison Result Among Different Methods

Method Name	**feature Dimension**	**Sen.**	**Spec.**	**Accu.**
Uniform LBP [23]	8	79.25%	94.56%	91.50%
Hist. probability [19]	6	83.00%	75.69%	77.15%
Intensity ratio [32]	4	94.78%	93.58%	94.00%
Stat (R/G) [28]	3	88.50%	96.63%	94.97%
Stat (Hue) [33]	4	93.08%	96.46%	95.24%
Stat (Y.I/Q) [34]	4	93.50%	94.00%	93.90%
Stat (CMYK) [27]	4	95.50%	92.87%	93.40%
Word hist. [22]	80	91.71%	94.05%	93.31%
Proposed RC & Stat	7	97.75%	97.99%	97.96%

2.3.4 Performance in Continuous WCE Video Clip

In this subsection, bleeding frame detection in continuous WCE video clip and the effect of post-processing step are demonstrated. For the purpose of analyzing performance in WCE video clip, five WCE bleeding videos are considered namely: 1) 'D170 bleeding', 2) 'bleding5', 3) 'bleeding3', 4) 'bleeding2', and 5) '23 bleeding', those are publicly available in [31]. Those videos are chosen in a way so that it covers different types of bleeding frame, as well as variation of frame number and position. First, from the video clip image frames are extracted and proposed final features are calculated. Then, bleeding and non-bleeding decision are acquired by applying SVM classifier and the performance is reported in Table. 2.6 and termed as without post-processing performance. Among the five videos, four videos show satisfactory performance in terms of all performance criteria, except 'bleeding3', due to the presence of numerous incidents of faint small bleeding areas. After getting primary bleeding detection result, post-processing algorithm is implemented. In the post-processing step, first, the decision of sequential frames in a video clip is tested, and applying necessary conditions an investigation zone is acquired. Examining feature distance from bleeding and non-bleeding frame of that investigation zone, a test non-bleeding frame can be toggled to bleeding, which is described in 2.1.5. As a result, a bleeding frame decision may be corrected, thus, the sensitivity is improved. The performance result of with and without post-processing are reported in Table. 2.6 in terms of sensitivity, specificity, and accuracy. It is shown from the table, the sensitivity, as well as accuracy, are significantly improved by post processing. In the case of 'bleeding3' video, its sensitivity is highly improved as well as accuracy. The overall result of considering all five videos are illustrated in Fig. 2.11. From the figure, it is clearly shown that the overall sensitivity and accuracy are improved by almost 4% and 2% respectively, which reflects strong justification of post processing step.

2.3.5 Experiment Results for Bleeding Zone Detection

Quantitative Analysis

A pixel-based comparison between the marked bleeding zone and the ground truth labeled by the clinicians is performed to measure the quantitative performance for

Table 2.6: Video Performance Result with Post Processing Effect

Video name	**Frames No. (B/N)**	**Criteria**	**Without post-proc.**	**With post-proc.**
D170 bl	96/4	sen.	98.97%	100.00%
		spec.	50.00%	50.00%
		accu.	97.00%	98.00%
bleeding5	22/78	sen.	86.36%	90.91%
		spec.	81.82%	90.91%
		accu.	96.15%	96.15%
bleeding3	5/95	sen.	60.00%	80.00%
		spec.	96.84%	96.84%
		accu.	96.00%	97.00%
bleeding2	100/0	sen.	100.00%	100.00%
		spec.	—	—
		accu.	100.00%	100.00%
23 bl	40/60	sen.	92.50%	95.00%
		spec.	98.63%	98.63%
		accu.	93.00%	94.00%

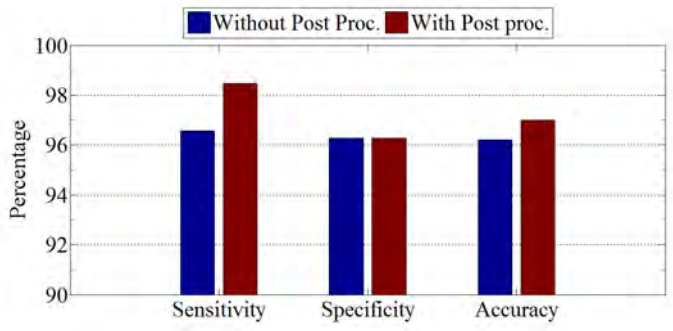

Fig. 2.11: Overall performance comparison between with and without post processing

detecting bleeding zone. The comparison result has four possible outcomes, they are true positive (TP), true negative (TN), false positive (FP) and false negative (FN). There are two true cases: 1) the bleeding pixels that are correctly labeled as the bleeding called true positive (TP) and 2) the non-bleeding pixels that are correctly labeled as non-bleeding termed as true negative (TN). Similarly, there are two false cases: 1) the pixels which are not labeled as the bleedings but should have been called false negative (FN) and 2) false positive (FP) are the ones incorrectly labeled as the bleedings. From those four outcomes three criteria are calculated to represent performance result as Precision, the false positive ratio (FPR) and false negative ratio (FNR) [35], [36], which is calculated according to the following

equations:

$$Precision = \frac{TP}{TP + FP} \tag{2.19}$$

$$FPR = \frac{FP}{FP + TN} \tag{2.20}$$

$$FNR = \frac{FN}{FN + TP} \tag{2.21}$$

Precision describes the truthfulness of bleeding zone detection, thus a higher value of it is highly desirable. In medical testing, more generally in binary classification, there are two types of errors as false positive and false negative. FPR and FNR represent those errors, hence, the lower value is considered better performance.

For the purpose of quantitative analysis, 100 bleeding images are tested, which are collected from 10 different bleeding videos. The ground truth of bleeding zone of those bleeding images is marked by the clinician. Bleeding zone detection result of different threshold values of proposed method is reported in Table. 2.7. Among the different performance parameters precession and the false negative ratio (FNR) are more crucial indicators. According to the definition of precision, FPR, and FNR; higher value of precision but the lower value of FNR and FPR are considered as a good result. FNR value represents failure detection percentage of the bleeding zone, which must be kept very low. As a result, high precision value and low FNR value are desired. Bleeding zone detection result of proposed method are reported in Table. 2.7 considering the variation of different threshold values. From the table, it is found that very high FNR value is obtained for lower threshold value. As threshold value is increased, FNR values are lower but precession values are drastically decreased. Thus, $T_{G/R}$ value should be set at a middle point; neither too large nor too small. From the table, the best performance result in terms of precession and FNR is obtained when $T_{G/R}$ value is kept less than equal 1/2.

For further analysis, proposed method of bleeding zone detection is compared with recently developed method reported in [22]. In [22], bleeding localization is marked by fusion strategy of two stage-salient maps considering 0.8 weighting of first stage-salient. The comparison result of bleeding detection performance is presented in Table. 2.8. From the table, it is clearly shown that the performance is significantly improved in terms of precision and FNR. Most important and significant improvement is observed in FNR ratio, which improved by almost 12%.

Table 2.7: Bleeding Zone Detection Performance of varying $T_{G/R}$ value

$T_{G/R}$ **value**	**Precession**	**FPR**	**FNR**
$T_{G/R} \leq 0.35$	88.27%	1.51%	80.84%
$T_{G/R} \leq 0.40$	90.37%	2.03%	70.25%
$T_{G/R} \leq 0.45$	89.69%	3.21%	48.95%
$T_{G/R} \leq 0.50$	**91.41%**	**6.23%**	**27.46%**
$T_{G/R} \leq 0.55$	86.63%	10.79%	13.96%
$T_{G/R} \leq 0.60$	78.24%	20.12%	5.38%
$T_{G/R} \leq 0.65$	65.41%	36.23%	2.46%

Table 2.8: Performance Comparison of Bleeding Zone Detection

Method	**Precession**	**FPR**	**FNR**
Yuan method [22]	88.20%	3.14%	39.60%
Proposed G/R threshold	**91.41%**	**6.23%**	**27.46%**

2.4 Conclusion

In this chapter, a new technique of bleeding frame and zone detection in wireless capsule endoscopy video recordings is presented. The proposed method exhibits high sensitivity, specificity and accuracy with respect to other established method. In the proposed method, red to green intensity ratio feature is explored. More discriminant feature quality is achieved between bleeding and non-bleeding images. In the proposed method, the best result of bleeding frame detection is obtained using ratio count and statistic feature in G/R domain as sensitivity 97.75% and accuracy 97.96%. It is observed that proposed post-processing algorithm improves bleeding frame detection performance by a significant margin. An automatic bleeding zone detection method is also presented with high precision. The proposed is thus promising in identifying bleeding zones from a bleeding image. In the future, we will develop more consistent and suitable feature for bleeding frame classification in order to archive the highest sensitivity.

Chapter 3

Proposed Unsupervised Cluster Based Bleeding Detection Scheme

In this Chapter, an efficient automatic scheme is proposed to identify the bleeding frames and zones from WCE video based on cluster specific feature (CSF). For the purpose of feature extraction, instead of using conventional red, green and blue (RGB) color plane, a transformed plane containing green to red pixel ratio is utilized. This helps in enhancing the separability between bleeding and non-bleeding pixels. Different statistical features are extracted from the overlapping spatial blocks of the preprocessed WCE image. The unique idea of the proposed method is to first perform unsupervised clustering of the extracted blocks to obtain two clusters and then extract global feature utilizing these CSFs along with differential cluster features. Finally utilizing the global feature, support vector machine (SVM) supervised classifier is employed to classify bleeding and non-bleeding images. It is found that the quality of the proposed CSF based global feature is significantly better than the feature extracted from the entire image. For bleeding frame detection in continuous WCE video data, a post-processing scheme is introduced utilizing the feature trends in neighboring frames. Finally using the CSF along with some morphological operations bleeding zones are identified. The proposed method is extensively tested on several WCE videos and a very satisfactory bleeding detection performance is achieved.

3.1 Introduction

The objective of this chapter is to develop an efficient computer aided bleeding frame and zone detection scheme in the WCE video recordings. In this Chapter,

starting from region level block based feature extraction, with the help of two class unsupervised clustering, an image level global feature is finally constructed to detect bleeding frames. From the given image, a transformed color plane utilizing green to red (G/R) pixel ratio is formed for extracting different statistical features in overlapping blocks. These blocks are first classified into two classes using unsupervised Kmeans clustering. Next global feature for an image is constructed by utilizing the cluster specific feature (CSF) along with the differential cluster feature. For the purpose of classification global features are used in SVM supervised classifier. A post-processing scheme utilizing neighboring frame characteristics is developed to detect bleeding frames from continuous WCE video data. Finally, the bleeding zones are detected by effectively utilizing the block labels. Simulation is carried out on several WCE video data. Our main contributions can be summarized in the following three aspects.

- A block-based local feature is extracted, which is considered more prominent representation instead of using individual pixel with respect to image noise, distortion and bleeding zone. While most of the literature consider individual pixel [25], [37], [22].

- An unsupervised classifier is used to segment WCE image into two clusters, which separates bleeding and non-bleeding regions, hence enhance global feature quality for detection of bleeding images.

- A bleeding zone detection algorithm is proposed using cluster segmentation which is acquired from the unsupervised classifier.

In order to obtain a quick overview of the proposed bleeding frame and zone detection method, in Fig. 3.1, a simplified block diagram is presented. From a given WCE video data, frame by frame feature extraction and classification tasks are carried out. Similar preprocessing and feature extraction operations are performed on both training and testing data. First, block-based statistical features are extracted from transformed G/R color plane. Next, an unsupervised Kmeans clustering method is employed on those blocks to obtain two clusters (cluster-I and cluster-II). Finally, a global feature vector is constructed using the cluster specific feature (CSF) extracted from each cluster and differential cluster features. The

global feature is used in supervised SVM classifier to detect bleeding images. In order to handle continuous video data, considering the classification results obtained on each frame, a post-processing operation on video segment is performed. Finally, a scheme for bleeding zone detection is carried out. In what follows, each step of the proposed method is described.

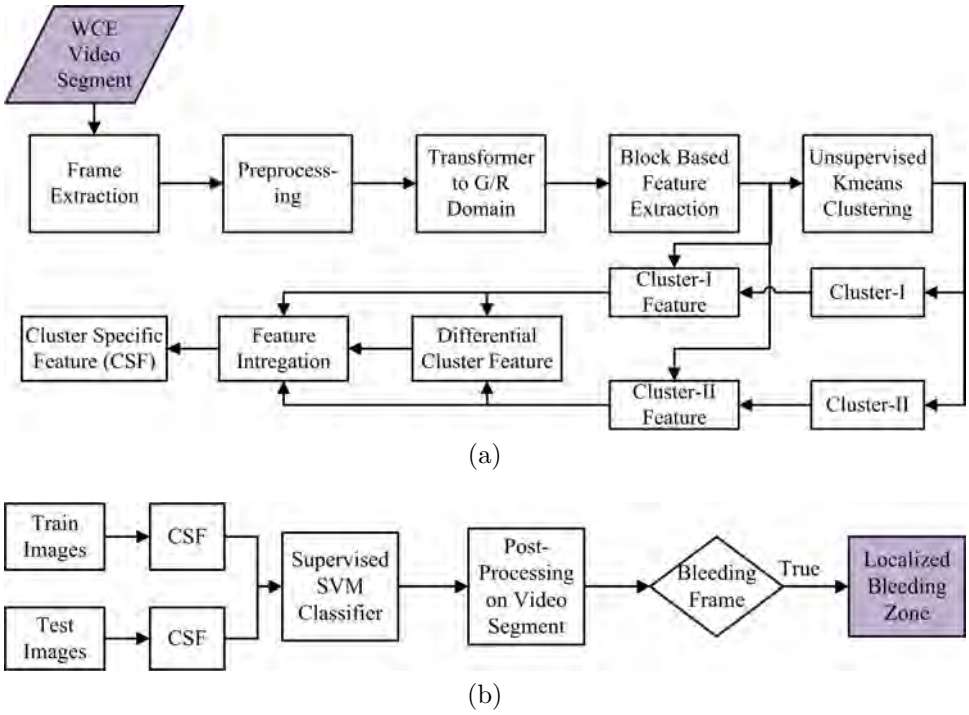

Fig. 3.1: Illustration of work flow of proposed method: (a) cluster specific feature (CSF) generation; (b) bleeding detection using CSF

3.2 Bleeding Frame Detection

3.2.1 Proposed Block Based Local Feature Extraction

Images in WCE video generally face different types of distortions due to motion blur and slow frame rate. Moreover, due to the inherent construction of gastrointestinal pathway, occlusion and changes in illumination may occur. As a result, there is a possibility that in a WCE image, an individual pixel may be corrupted or distorted. In most of the bleeding detection methods, the analysis is carried out on pixel level, i.e. features are extracted from each pixel [25], [37], [22]. In this case, there is a chance that the consistency of extracted features will be poor if there are some distorted pixels in a WCE image. In order to overcome this problem, instead of computing features from an individual pixel, we propose to consider the

neighborhood block of that pixel for feature computation. Since in general, even a very small bleeding zone consists of several pixels, it is expected that such block based feature extraction can overcome the problem of single pixel distortion and offer feature consistency. Moreover, depending on the amount of overlap between consecutive blocks, block based feature extraction may reduce the computational burden. For example, in an image with $M \times M$ pixels, if pixel values are directly considered as a feature, feature dimension would be M^2. If feature extraction is performed on $m \times m$ non-overlapping blocks, in total $J \times J$ blocks will be required, where $J = floor(M/m)$. In this case, if the average value of each block is considered as feature, J^2 average values containing local information can be used to construct feature vector with dimension $J^2 < M^2$. It is to be mentioned that although only J^2 blocks instead of M^2 pixels are used, in each block, all pixels are utilized to extract feature. Thus, conventional pixel down-sampling operations are not equivalent to block based feature extraction. In Fig. 3.2, a WCE image in composite G/R plane is shown from which a sample square block with a dimension 5×5 pixels is marked. This type of spatial blocks is used for feature extraction.

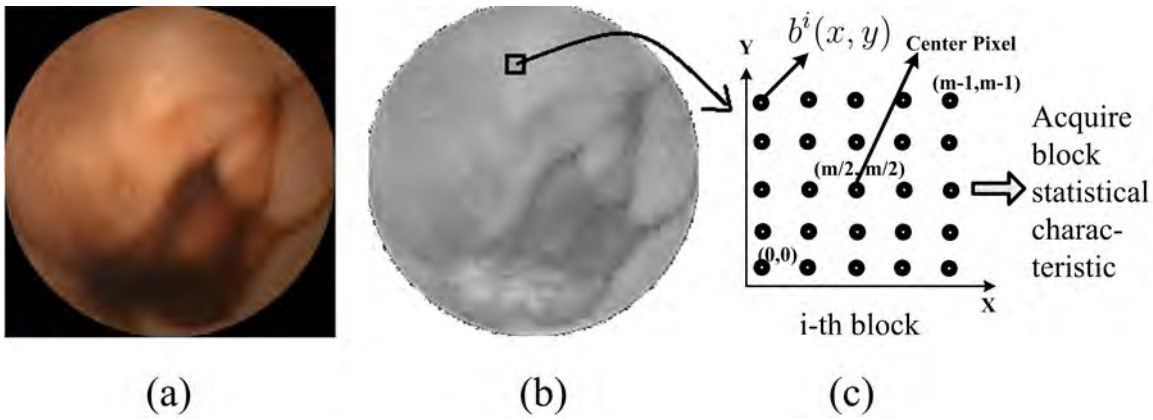

Fig. 3.2: Representation of neighborhood block characteristic (a) given image; (b) G/R composite plane; (c) a sample block of size 5×5 pixels and statistical characteristics

In view of obtaining spatial characteristics of each block, conventional statistical parameters are computed, such as mean, median, maximum, minimum, intensity of block center, and difference between block-mean and block center intensity. For $m \times m$ dimensional i-th block with pixel intensities $b^i(x, y)$, statistical measures namely mean (B^i_{mean}), median (B^i_{median}), max (B^i_{max}), min (B^i_{min}) are computed.

Moreover, deviation of center pixel value from the block mean value is also taken into consideration. This defined as

$$B^i_{diff} = |B^i_{mean} - B^i_C| \tag{3.1}$$

where, B^i_C represents center pixel intensity of i-th block which is centered at $(m/2, m/2)$ (shown in the Fig. 3.2 (c) and the mean value of i-th block ($m \times m$ size) is computed as

$$B^i_{mean} = \frac{1}{m \times m} \sum_{x=1}^{m} \sum_{y=1}^{m} b^i(x, y) \tag{3.2}$$

Finally a feature vector for i-th block is constructed as

$$\mathbf{f}^i = [B^i_{mean}\ B^i_{median}\ B^i_{max}\ B^i_{min}\ B^i_{diff}\ B^i_c], \quad i \in all\, blocks \tag{3.3}$$

This block based features are treated as regional features, which will be directly used in an unsupervised clustering scheme to obtain preliminary two class classification among the pixels of given WCE image.

3.2.2 Proposed Method of Global Feature Extraction

In order to classify bleeding and non-bleeding images, a representative feature from a given WCE image needs to be extracted by utilizing features computed from all blocks. If all the block features, extracted from a given image, are combined, the feature dimension would be extremely large and it may not exhibit a consistent pattern. One possible solution is to develop a global feature for each image by utilizing features extracted from all blocks. However, quality of the global feature will depend on the size of the bleeding and non-bleeding regions in WCE image. For example, in some bleeding images, there may be a large non-bleeding region. In this case, if the global feature is extracted by using features of all the blocks, it may not be capable of representing the bleeding image because of the dominance of non-bleeding blocks. In order to overcome this problem, we propose to segment a given image into two possible regions and then extract global features from each region separately. As a result, from a given image, instead of one feature vector, two feature vectors will be obtained from two regions, which will be concatenated to get the desired feature. It is expected that the feature vector extracted from each region will offer better consistency, no matter whether it is a bleeding or non-bleeding

image. In particular, the advantage will be very prominent in the case of bleeding images where the two regions belong to two different classes. Two major concerns in the proposed method of global feature extraction are: the process to be used for segmentation of the image and the method of extracting proposed concatenated feature. In what follows, two major steps related to these two concerns are presented in detail.

Unsupervised Two Class Clustering

The objective at this stage is to segment a given image into two regions for an extracting consistent global feature from each region. In the case of bleeding image, it is expected that the two segments will belong to bleeding and non-bleeding regions. In the case of non-bleeding images, the two segments will exhibit very similar characteristics, as both of them belong to same class (non-bleeding region). Hence, there are two possibilities when a test image is segmented into two clusters: (1) both segments belong to the non-bleeding region and (2) one bleeding and one non-bleeding region. Depending on some discriminative characteristics, two clusters and corresponding cluster labels (I or II) need to be obtained. Since the objective here is to obtain two clusters, block based features (block statistical parameters) described in the previous sub-section can be used for this purpose. In this regard, one may utilize a supervised or unsupervised classifier. Considering a large number of blocks available in each image and their variations, constructing a representative train dataset for different types of blocks would be a cumbersome job. As a result, instead of the supervised classifier, an unsupervised clustering method is employed to obtain the two segments. Among different available clustering schemes, K-means clustering is considered for unsupervised classification, which is found very suitable for handling a large amount of data. K-means clustering is the most widely used partitioning method that can segment the given dataset into K mutually exclusive clusters and mark each cluster by an index number. For the two-class clustering required in the proposed method, K-means will determine a partition dividing the dataset into two clusters (C_I and C_{II}) where members within each cluster are as close to each other as possible, and as far from the members in other clusters as possible. In the K-means clustering, block statistical parameters described in (3.3) are used as features, namely mean, median, maximum, minimum, intensity of the

center pixel of a block B_c, and the deviation of center pixel value from the block mean value are employed as features. It is observed that for the bleeding image K-means exhibits satisfactory performance in separating bleeding zone from the non-bleeding neighborhood. On the other hand, for non-bleeding images, K-means creates two clusters as dominant and less dominant non-bleeding zones. A sample clustering outcome obtained by using the K-means is shown in Fig. 3.3 considering one bleeding and one non-bleeding image. In Fig. 3.3 (a), a bleeding image and in Figs. 3.3 (b) and (c), corresponding two clusters (C_I and C_{II}) are shown. From this figure, it is observed that the bleeding and non-bleeding zones are satisfactorily separated in clusters I and II. Similarly, the clustering of a non-bleeding image is demonstrated in Figs. 3.3 (d)-(f). It is observed in this figure that the K-means clustering attempts to ensemble blocks exhibiting very similar characteristics in one cluster. Next, for both clusters, mean pixel intensities (I^I_{avg}, I^{II}_{avg}) are computed. Each these two intensities can easily be obtained by average the block mean values of a particular cluster and can be expressed as

$$I^I_{avg} = \frac{1}{N_I} \sum_{i \in C_I} B^i_{mean} \tag{3.4}$$

$$I^{II}_{avg} = \frac{1}{N_{II}} \sum_{j \in C_{II}} B^j_{mean} \tag{3.5}$$

In view of obtaining consistency in cluster labeling, in the proposed method between the two clusters, a cluster with lower I_{avg} is marked as cluster-I. For labeling a cluster, it is found that considering only one feature statistics above is sufficient. Next from those two clusters, global features are calculated using block features and this global feature will be used in the supervised classifier to declare a frame as bleeding or non-bleeding.

Concatenating Cluster Based Features

In global feature extraction, one may consider only one cluster of a given image. For example, only cluster-I may be considered, which consists of lower centroid value of the mean feature. In this case, for bleeding images it is expected that the cluster-I corresponds to a bleeding zone in the G/R transform plane. However, the problem will arise in testing the non-bleeding images, where considering global

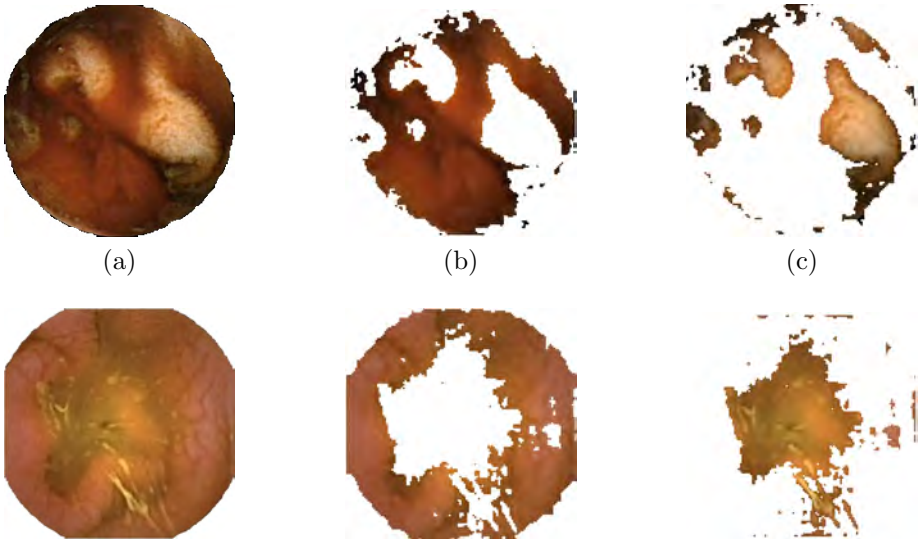

(a) (b) (c)

(d) (e) (f)

Fig. 3.3: Illustration of segmentation of clustering (a) WCE bleeding frame; (b) cluster-I from bleeding frame; (c) cluster-II from bleeding frame; (d) WCE non-bleeding frame; (e) cluster-I from non-bleeding frame; (f) cluster-II from non-bleeding frame

feature extracted only from cluster-I may lead to introduce bias in declaring a non-bleeding image as bleeding. As a result of the proposed method, features extracted from both clusters are used in the final stage of bleeding and non-bleeding image classification. From each cluster, centroid of the block features is computed which results in six-dimensional feature vector given by

$$\mathbf{F}_I = \frac{1}{N_I} \sum_{i=1}^{N_I} \mathbf{f}^I, \quad i \in C_I \tag{3.6}$$

$$\mathbf{F}_{II} = \frac{1}{N_{II}} \sum_{j=1}^{N_{II}} \mathbf{f}^j \quad j \in C_{II} \tag{3.7}$$

where N_I and N_{II} is the number of blocks in C_I and C_{II}, respectively. Since natural images are used, it is obvious that features extracted from the two clusters will exhibit some differences, no matter whether it is bleeding or non-bleeding image. Apart from using, $\mathbf{F}_I$ and $\mathbf{F}_{II}$ vectors, one interesting idea is to introduce a differential feature vector, defined as

$$\mathbf{F}_{diff} = |\mathbf{F}_I - \mathbf{F}_{II}|. \tag{3.8}$$

It is expected that $\mathbf{F}_{diff}$ is significantly lower in the case of non-bleeding images than those of the bleeding images. Because of the strong distinguishable characteristics,

use of this differential feature can help in obtaining better classification performance. Hence, the desired feature vector to be used for image classification is proposed as

$$\mathbf{F}_{final} = [\mathbf{F}_I \ \mathbf{F}_{II} \ \mathbf{F}_{diff}]. \tag{3.9}$$

This global feature is termed as cluster specific feature (CSF) which is used in a supervised classifier to carry out the two class image classification.

Feature Quality

There is no doubt that the overall bleeding detection performance strongly depends on the quality of the extracted CSF. One commonly used tool to demonstrate the quality of the extracted features in terms of statistical parameters is the box plot. In box plot representation, box edges are 25th and 75th percentiles, whereas central mark is the median of a given data. The most extreme data points are the whiskers, and outliers are plotted individually [38]. In Fig. 3.4, box plot representation of proposed CSF is demonstrated considering 200 bleeding and 200 non-bleeding images. In Figs. 3.4 (a)-(f), in each box, statistical behavior of four variables is shown. First, two variables of each box correspond to the behavior of a particular CSF extracted from cluster-I of bleeding and non-bleeding images denoted as cluster-I(B) and cluster-I(N), respectively. Similarly, second two variables represent the behavior corresponding to cluster-II denoted as cluster-II(B) and cluster-II(N), respectively. For each of the six features, the centroid of the block features in each cluster is computed. Feature extracted from non-bleeding images provide very high within class compactness and as expected in this case, the difference in the cluster centroids of two clusters is very small. For some features cluster-I provides better separation between bleeding and non-bleeding classes (e.g. Figs. 3.4 (b), (d), (f)), while for some other features cluster-II provides better class separation (e.g. Figs. 3.4 (a), (c), (e), (f)). As a result, both clusters features are taken into consideration in proposed CSF. Moreover, it is observed in the figure that class separation becomes significantly high when differential cluster feature is used (Figs. 3.4 (h)-(l)), except for one case Fig. 3.4 (g). . It can be inferred from the figures, that proposed feature values exhibit significant separation between two classes with a very few exception.

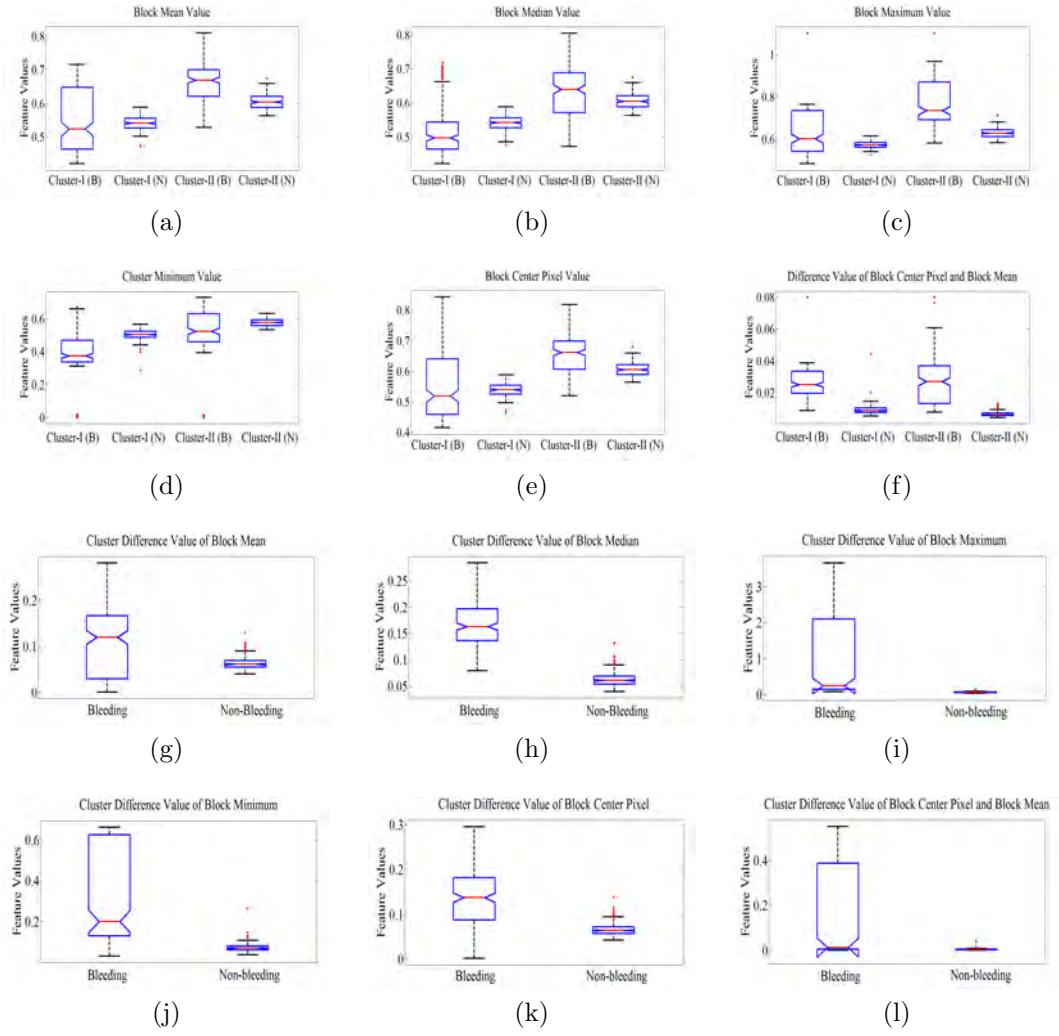

Fig. 3.4: Feature quality analysis (a) Box plot of cluster mean; (b) Box plot of cluster median; (c) Box plot of cluster maximum; (d) Box plot of cluster minimum; (e) Box plot of block center pixel; (f) Box plot of difference between center pixel and mean of block; (g) Box plot of difference of cluster mean; (h) Box plot of difference of block cluster median; (i) Box plot of difference of cluster maximum; (j) Box plot of difference of cluster minimum; (k) Box plot of difference of cluster center pixels; (l) Box plot of cluster difference of difference between center pixel and mean of block

3.2.3 Post-Processing

In previous subsections, a complete method of classifying a test WCE image as bleeding or non-bleeding is proposed. In the WCE based diagnosis, generally the objective is to find out the bleeding frames in a WCE video recording. In this case, each frame of a given WCE video needs to be tested. Thus, temporal information of videos (consecutive frame sequence) is available. In order to improve bleeding frame detection performance, a post-processing algorithm is developed using that temporal information. At first, an investigation zone is selected, which is same as

section 2.1.5. Then, image that are labeled as non-bleeding are rechecked by feature distance based criteria.

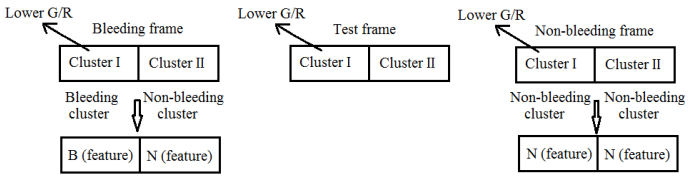

Fig. 3.5: Illustration of post processing scheme

As described before, from each image two sets of global features are extracted from the two clusters. For the purpose of rechecking a distance based criteria using CSF is proposed. At first, the number of bleeding and non-bleeding images is counted in an investigation pool while ignoring the test non-bleeding image. Let the total number of bleeding and non-bleeding labeled images are P and Q respectively. There are two possibilities: $Q = 0$ and $Q \neq 0$. For the first case ($Q = 0$), it is more logical that the test image may be labeled falsely as non-bleeding as there are no non-bleeding images nearby that test image. In this case without further calculation, the test non-bleeding image is declared as bleeding. In second case ($Q \neq 0$), for the purpose of rechecking centroid feature extracted from cluster-I ($\mathbf{F}_I$) is considered. Mean absolute difference (MAD) between $\mathbf{F}_I$ extracted from the test image ($\mathbf{F}_{I_T}$) and $\mathbf{F}_I$ obtained from bleeding images ($\mathbf{F}_{I_B}$) is defined as

$$D^b = \frac{1}{P}\sum_{i=1}^{P} |\mathbf{F}^i_{I_B} - \mathbf{F}_{I_T}| \tag{3.10}$$

Similarly MAD between ($\mathbf{F}_{I_T}$) and $\mathbf{F}_I$ obtained from non-bleeding images ($\mathbf{F}_{I_N}$) is defined as

$$D^n = \frac{1}{Q}\sum_{j=1}^{Q} |\mathbf{F}^j_{I_N} - \mathbf{F}_{I_T}| \tag{3.11}$$

To take the final decision, whether the label of the test frame need to be changed or not, conditions are same as described in section 2.1.5.

3.3 Bleeding Zone Detection

In this section, identification of bleeding regions in detected bleeding frames is presented. In the proposed method, first, with the help of unsupervised classifier,

different blocks in a given image are classified into two clusters (cluster-I and cluster-II) and then feature based supervised classifier is used to identify bleeding (B) or non-bleeding (N) images. Next, bleeding zone detection will be carried out only on bleeding images. Each block of a bleeding image is already marked as cluster-I or cluster-II. One of this two cluster corresponds to the bleeding region and the other one corresponds to the non-bleeding region. Since each pixel of a bleeding image needs to be identified, it will be helpful if only the clusters correspond to the bleeding region is considered. Hence, first, the task is to find the label (bleeding or non-bleeding) of each cluster and then carry out bleeding zone detection algorithm on each pixel of a bleeding cluster. Major steps, to be performed in the proposed bleeding zone detection algorithm are given below

- Determining the label of two clusters of an image whether bleeding or non-bleeding
- Determining the label of each pixel in a block whether bleeding or non-bleeding
- Fine tuning of bleeding zone with the help of morphology operation.

3.3.1 Determining the Label of Cluster

During performing unsupervised clustering of the blocks of a given WCE image, several features, extracted from a block, are utilized. However at this stage, the objective is not to further classify the blocks into two classes rather finding the bleeding cluster between the available two clusters. Thus considering all those features are not necessary for this purpose. It is observed that bleeding pixels exhibit higher red (R) but lower green (G) intensity values with respect to non-bleeding pixels. As a result, in the G/R composite plane, pixel intensity ratio is lower for the bleeding pixels than that of non-bleeding pixels. If the mean value of G/R pixel intensity ratio, computed within a block, is considered, it is expected that the blocks in a bleeding cluster will exhibit on average lower values in comparison to those in the non-bleeding clusters. For better understanding, an average of mean G/R values of all the blocks in bleeding cluster and that of non-bleeding clusters are computed for 100 bleeding images and the results are shown in Fig. 3.6. In the figure, it is clearly observed that for every bleeding image, an average of mean G/R values is lower for

bleeding cluster than that of non-bleeding clusters. Hence, in order to determine the label of a cluster, in the proposed method, the average of mean G/R values of each of the two clusters is considered and the cluster having lower average value is termed as a bleeding cluster and other is termed as a non-bleeding cluster. The bleeding cluster is a combination of blocks and in general, it is assumed that all the blocks of a bleeding cluster are labeled as bleeding. Similarly, for the non-bleeding cluster, all the blocks are labeled as non-bleeding.

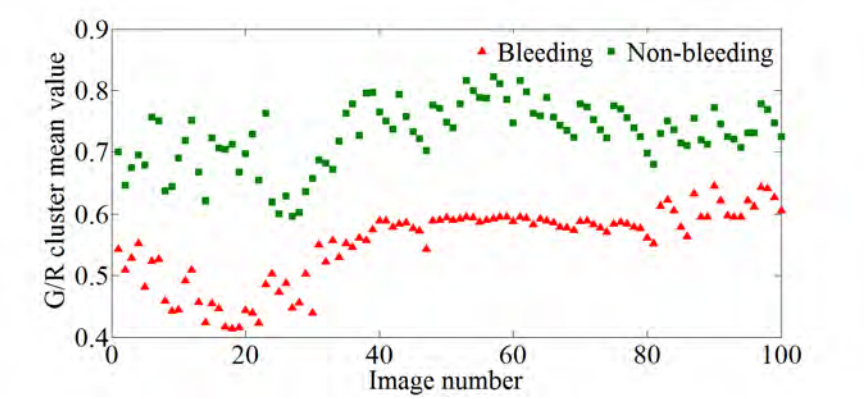

Fig. 3.6: Illustration of cluster mean value of green to red ratio for bleeding and non-bleeding cluster

3.3.2 Determining the Label of Pixel

After getting the marking of all the blocks, our objective is to determine the label of each pixel in a block. One of the possible solutions is to label all the pixels of a block same as the block label, however, each block consists several pixels and all the pixels may not necessarily belong to same class. Especially, in the case of overlapping blocks, one pixel may have more than one labels when it belongs to different blocks with different labels. In these cases, it would be very difficult to take the final decision on those overlapping pixels. Therefore, in order to find a suitable method to detect bleeding zone, in the proposed method, a pixel based interpolation technique is developed.

At first for a test pixel, its membership status is determined by using the number of blocks which contain that particular test pixel. Considering 3×3 block size with 33% overlapping, in Fig. 3.7(a), 16 blocks are shown. A pixel can be a member of one or several blocks and can be termed as center pixel (o), arm pixel (ap) and corner pixel (cp) depending on its location in a block. In this figure, each center pixel of

a block (marked as circular blue) is a member of only one block, with membership count 1. The arm pixel (marked as diamond yellow with AP) is a member of two blocks (according to the figure, its left and right blocks or up and down blocks), thus, its member count is 2. And the corner pixel (marked as diamond yellow with CP) is a member of four surrounding blocks (according to the figure), thus, its membership count is 4. In the second step, labels of membership blocks are taken into consideration to obtain the label of a test pixel. For taking final decision of a test pixel with membership value n, preliminary labels of n number of blocks need to be considered. The label of the test pixel is finalized depending on the majority voting principle, that is, if higher than $\frac{n}{2}$ blocks belong to bleeding class, the test pixel is declared as bleeding. But in the case of equal ($\frac{n}{2}$) bleeding and non-bleeding belonging blocks, then it is quite a difficult task to take an accurate decision and this problem is called 'no majority found'. To overcome this problem, in this research, a region growing surrounding block based method is proposed. If a test pixel belongs to an equal number of bleeding and non-bleeding blocks, first tire surrounding blocks are considered and again check the majority voting of those surrounding blocks to mark that test pixel. If first tire surrounding blocks face same 'no majority found' problem, second tire surrounding blocks will be taken into consideration and so on. This pixel-wise proposed method is executed in the whole image and considered more suitable to take acceptable decision for the test pixel. In Fig. 3.7(b), a case is presented where red boundary blocks are bleeding blocks and green boundary blocks are non-bleeding blocks. In this case, the boundary of bleeding and non-bleeding clusters faces problem to determine the appropriate label of the pixels, but that problem is solved using proposed method, corner pixel (marked as CP in the figure) is marked using block membership count of that pixel and its block decisions. Here corner pixel is a member of four surrounding blocks, three of the four blocks decision is bleeding so that test corner pixel is labeled as bleeding according to the proposed method that relies on majority voting decision rule. While considering AP marked arm pixel (as shown in the figure), its block membership count is two. One of the blocks is marked as bleeding and another one as non-bleeding, so majority rule fails to determine the label of that pixels, as a result, first tire surrounding blocks are considered for decision making. Here, 10 surrounding blocks are available, among

the 10 blocks 3 are labeled as non-bleeding and 7 are labeled as bleeding, thus, the test arm pixel finally marked as bleeding (red diamond). Applying proposed a method, all the pixel in Fig. 3.7(b) are marked, here red and green color represent bleeding and non-bleeding pixel respectively.

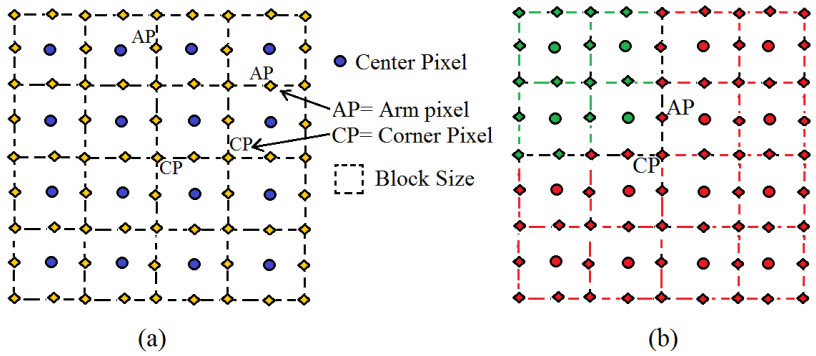

Fig. 3.7: Demonstration of pixel marking for bleeding zone detection

3.3.3 Fine Tuning of Bleeding Zone Using Morphology Operation

Fine tuning of bleeding zone is described in section 2.2.1.

3.4 Simulation and Experimental Result

3.4.1 Performance of Bleeding Image Detection

Parameter Selection

First, after applying preprocessing technique described in subsection 2.1.1, black-boundary pixels are eliminated from given WCE images. Then, the G/R transformed plane is constructed by using the pixel intensity ratio of red and green planes (refer to subsection 2.1.2). Next, for block-based local feature extraction, as described in subsection 3.2.1, blocks are constructed and effect of variation of block size and percentage overlapped on bleeding, detection performance is investigated. Performance evaluation results are reported considering three different block sizes: 3×3, 5×5, 7×7 and 9×9 with various combinations of overlapping. Different local features, such as mean, median, maximum, minimum and center pixel values of the block, and the distance between the center pixel value and block mean value are calculated. For the purpose of segmentation, K-means clustering is employed as an

unsupervised classifier, and local features are used as a feature vector to segment a given image into two clusters. Cluster wise global features are calculated and hence, the final feature vector is formed as described in subsection 3.2.2. For bleeding frame, classification SVM classifier is used with different kernel functions, such as the linear kernel and radial basis function (RBF) kernel. Experimental performance is evaluated based on 10 fold cross validation technique.

Performance of Bleeding Frame Detection

In this subsection, the performance of the bleeding frame detection obtained by the proposed method is presented in terms of accuracy, sensitivity and specificity. Here the effect of different parameters, such as block size, overlapping between blocks, and types of the classifier are taken into consideration. In Table 3.1, the effect of variation of block size on the performance of bleeding detection is presented considering 3×3, 5×5, 7×7 and 9×9 block dimensions using SVM classifier with radial basis function (RBF) kernel. From detailed investigation on severe bleeding and non-bleeding blocks, it is found that in comparison to the whole bleeding area, a very small sized block may not represent a significant area of bleeding. On the other hand, a large sized block may contain both bleeding and non-bleeding regions. As a result, it is more suitable to take the moderate size of the block to obtain the best bleeding detection performance. This fact can be visualized from the results shown on from Table 3.1. It is observed from the table that the value of all three performance indicators increases with the increase in block size starting from 3×3 up to 7×7 and after that further increase in the block size to 9×9 causes decrease in the performance.

Table 3.1: The Effect of Block Size on Bleeding Frame Detection Performance

Block Size	**Sensitivity**	**Specificity**	**Accuracy**
3 by 3	93.28%	97.29%	96.39%
5 by 5	94.86%	97.44%	96.83%
7 by 7	95.70%	97.94%	97.49%
9 by 9	94.79%	96.85%	96.11%

It is to be mentioned that one major contribution of this proposed method is the cluster based feature extraction. In order to demonstrate the effect of unsupervised clustering used in the proposed method on classification performance, in

Fig. 3.8, comparative performance analysis is shown considering with and without clustering. In the figure, different size of blocks is considered to demonstrate the bleeding detection performance in terms of sensitivity, specificity and accuracy. As discussed before, it is expected that better classification performance is achieved when features are extracted from after unsupervised clustering. This fact is clearly observed in the figure, where the result obtained with clustering found superior to the case where features are extracted from the whole image without any clustering.

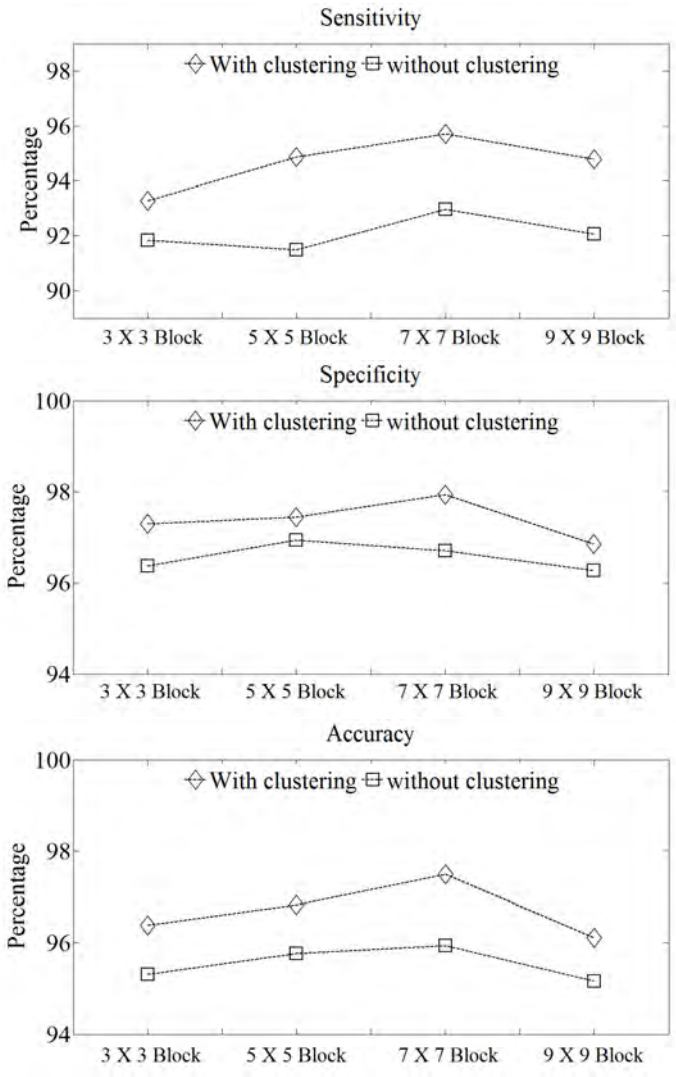

Fig. 3.8: Classification performance effect of clustering

Next, the effect of changing percentage of overlap between consecutive blocks is investigated and the results are reported in Table. 3.2. In that table, only 5×5 and 7×7 block dimensions are considered due to their high level of performance observed in Table. 3.1. Here 0%, 20% and 40% overlap between two consecutive blocks of 5×5 size and 0%, 14%, 28% and 43% overlap between two consecutive blocks of

7×7 size are taking into consideration. More than 50% overlap between two consecutive blocks is not considered. It is observed that, overlapping block scheme is more suitable to overcome single pixel randomness and distortion problem, hence offers better feature consistency than non-overlapping block feature. Thus, overlapping block scheme performed better than a non-overlapping block. It is observed that in comparison to the non-overlapping scenario if small overlapped between consecutive two blocks is allowed, a significant improvement of all performance criteria is achieved. However, considering a large amount of overlapped may not necessary improve the performance characteristics. For example, in the case of 7×7 block size, best performance is obtained by considering 14% overlapped.

Table 3.2: The Effect of Block Overlapping on Bleeding Frame Detection Performance

Block Size	**Overlapping Percentage**	**Sensitivity**	**Specificity**	**Accuracy**
5by 5	0%	94.86%	97.44%	96.83%
5 by 5	20%	95.09%	97.83%	97.32%
5 by 5	40%	94.80%	97.74%	97.12%
7 by 7	0%	95.70%	97.94%	97.49%
7 by 7	14%	96.22%	98.54%	98.04%
7 by 7	28%	95.25%	98.11%	97.53%
7 by 7	43%	95.67%	97.80%	97.36%

Furthermore, bleeding detection performance is investigated using different types of classifiers using the final proposed feature and results are presented in Table 3.3 considering LDA, KNN and SVM classifier. For KNN classifier, the value of k is varied from 1 to 10 and the value of k for which the best performance in terms of sensitivity is achieved is reported in Table 3.3.

Table 3.3: The Effect of Classifier on Bleeding Frame Detection Performance

Classifier	**Sensitivity**	**Specificity**	**Accuracy**
LDA	95.79%	97.85%	97.45%
KNN	95.86%	97.54%	97.19%
SVM	96.22%	98.54%	98.04%

Bleeding detection is a two class problem and it is well known that SVM classifier is better suited for this type of problem, which is also reflected in the results shown in Table. 3.3. Here for SVM classifier, the radial basis function (RBF) kernel is used.

In SVM classifier, different kernels are tested and the effect of variation of kernels on bleeding detection performance is reported in Table. 3.4, considering 7×7 block size with 14% overlap. It is observed that in comparison to linear and polynomial kernels, RBF kernel provides better classification performance in terms of all three performance measurement criteria.

Table 3.4: The Effect of SVM Kernel on Bleeding Frame Detection Performance

Kernel	**Sensitivity**	**Specificity**	**Accuracy**
Linear	92.24%	97.01%	96.51%
Polynomial	93.86%	97.74%	96.83%
RBF	96.22%	98.54%	98.04%

Performance Comparison with Established Method

In view of comparing the performance of the proposed method, eight recently reported methods are taken into consideration [23], [19], [32], [28], [27], [33], [34] and [22]. One common approach to bleeding detection is the use of Local Binary Pattern (LBP) [23] based feature. In LBP based method 8 bin histogram is used for feature extraction. The method reported in [22] utilizes 80 bin word based color histogram for feature extraction. In [19], bleeding detection is performed using color features from histogram probability. In implementing the method reported in [19], the best feature combination as mentioned in the chapter is taken into account. the other two methods [32], [28], chosen for performance comparison utilize statistical feature extracted from each pixel of WCE image. Comparison results are presented in Table. 3.5. For a fair comparison, same WCE image dataset and classifier are used for all these eight methods. It is to be noted that proposed method is named as CCBF (cluster centroid of block feature). It is observed that proposed method exhibits superior performance to all other reported methods, in terms of all performance indicators. It is observed that performance of proposed method is significantly improved in terms of sensitivity. The possible reasons for getting superior classification performance by the proposed method are its capability of overcoming some difficulties commonly observed in WCE images, such as single pixel randomness, illumination changes, and image distortion. Another reason is the consistency of the proposed feature that does not depend on the size of the bleeding zone.

Table 3.5: Performance Comparison of Different Features

Method Name	**Sen.**	**Spec.**	**Accu.**
Uniform LBP [23]	79.25%	94.56%	91.50%
Hist. probability [19]	83.00%	75.69%	77.15%
Intensity ratio [32]	94.78%	93.58%	94.00%
Stat (R/G) [28]	88.50%	96.63%	94.97%
Stat (Hue) [33]	93.08%	96.46%	95.24%
Stat (Y.I/Q) [34]	93.50%	94.00%	93.90%
Stat (CMYK) [27]	95.50%	92.87%	93.40%
Word hist. [22]	91.71%	94.05%	93.31%
Proposed CCBF	96.22%	98.54%	98.04%

3.4.2 Performance in Continuous WCE Video Clip

In this subsection, the outcome of post processing step alone with bleeding frame detection performance in continuous video segment are described. In order to inspecting the performance in WCE video clip, five WCE bleeding videos are tested namely: 1) 'D170 bleeding', 2) 'bleding5', 3) 'bleeding3', 4) 'bleeding2', and 5) '23 bleeding', those are widely accessible in [31]. Those videos are selected so that they offer variation in bleeding frame number and position in a video. First, from the video clip image frames are extracted and proposed final features are computed. Then, the decision of test frame is acquired by applying SVM classifier and the performance is reported in Table. 3.6 and named as without post-processing performance. Among the five videos, four videos show satisfactory performance in terms of all performance criteria, except 'bleeding3', due to the presence of numerous incidents of faint small bleeding areas.

After getting primary bleeding detection result from the supervised classifier, post-processing algorithm is implemented. In the post-processing step, first, frame decision of video clip sequence is tested with certain conditions and acquired an investigation zone centering a frame which is primarily labeled as non-bleeding. Fulfilling necessary condition a test non-bleeding frame can be toggled to bleeding, which is described in 3.2.3. Therefore, a bleeding frame decision may be corrected, thus, the sensitivity is improved. The performance result of with and without post-processing are reported in Table. 3.6 in terms of sensitivity, specificity, and accuracy. As expected, the sensitivity, as well as accuracy, is significantly improved by post processing. In the case of 'bleeding3' video, its sensitivity is highly improved as well

as accuracy. The overall result of considering all five videos are illustrated in Fig. 3.9. From the figure, it is clearly shown that the overall sensitivity and accuracy are improved by almost 4% and 2% respectively, which reflects strong justification of post processing step.

Table 3.6: Video Performance Result with Post Processing Effect

Video name	**Frames No. (B/N)**	**Criteria**	**Without post-proc.**	**With post-proc.**
D170 bl	96/4	sen.	91.87%	93.75%
		spec.	100.00%	100.00%
		accu.	92.00%	94.00%
bleeding5	22/78	sen.	86.36%	90.91%
		spec.	94.87%	94.87%
		accu.	93.00%	94.00%
bleeding3	5/95	sen.	80.00%	100.00%
		spec.	97.87%	97.87%
		accu.	97.00%	98.00%
bleeding2	100/0	sen.	96.00%	99.00%
		spec.	—	—
		accu.	96.00%	99.00%
23 bl	40/60	sen.	90.00%	97.50%
		spec.	88.33%	88.33%
		accu.	89.00%	92.00%

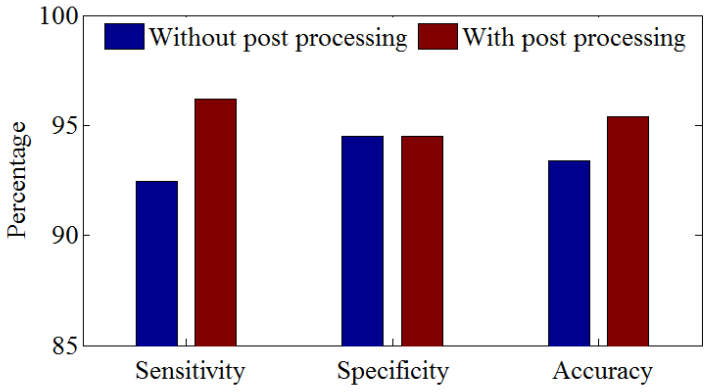

Fig. 3.9: Overall performance comparison between with and without post processing

3.4.3 Experiment Results for Bleeding Zone Detection

Quantitative Analysis

For the purpose of quantitative analysis, 100 bleeding images are tested, which are collected from 10 different bleeding videos. The ground truth of bleeding zone of

those bleeding images is marked by the clinician. Bleeding zone detection result of a different parameter of proposed method are reported in Table. 3.7. Among the different performance parameters precession and the false negative ratio (FNR) is a more crucial indicator. According to the definition of precision, FPR, and FNR; higher value is of precision but the lower value of FNR and FPR are considered as a good result. FNR value represents failure percentage of bleeding zone detection, which must be kept very low. As a result, high precision value and low FNR value are expected. Bleeding zone detection result of proposed method are reported in Table. 3.7 considering variation of different block sizes. 3×3, 5×5, 7×7 and 9×9 block dimensions are investigated and found that very small size of the block could not represent a significant area of bleeding, on the other hand, big size of the block may contain both bleeding and non-bleeding regions. As a result, it is more suitable to take the moderate size of the block to obtain the best performance result. Hence, in terms of precision, better performance result is obtained considering 7×7 block size. It is noted that bleeding zone detection performance highly depends on local block features, which are used for segmenting bleeding and non-bleeding zone as mentioned in 3.2.2.

Table 3.7: Bleeding Zone Detection Performance of Different Block Size

Method	**Precession**	**FPR**	**FNR**
3 by 3 block	94.21%	2.71%	24.85%
5 by 5 block	96.11%	1.46%	28.23%
7 by 7 block	**96.81%**	**1.28%**	**33.37%**
9 by 9 block	96.17%	1.52%	42.98%

Different types of overlapping blocks are investigated and reported in Table. 3.8. In that table, only 5×5, and 7×7 block dimensions are considered due to their high-performance potential. 0%, 20% and 40% overlap between two consecutive blocks of 5×5 size and 0%, 14%, 28% and 43% overlap between two consecutive blocks of 7×7 size are taking into the investigation. More than 50% overlap between two consecutive blocks is not considered. It is observed that, overlapping block scheme is more suitable to overcome single pixel randomness and distortion problem and offers consistency of local block feature. Thus, overlapping block scheme performed better than a non-overlapping block. Performance result is also varied due to an overlapping percentage between adjacent blocks. In order to examine the effect of

overlapping percentage between two adjacent blocks; 14%, 28% and 43% overlapping of 7×7 blocks are considered and found that, if a large portion of a block is overlapped, local feature quality of blocks are degraded as well as the bleeding zone detection performance. As a result, in terms of precision, the best performance is obtained from 14% overlapping block of 7×7 size which is shown in Table. 3.2.

Table 3.8: The Effect of Block Overlapping on Bleeding Zone Detection Performance

Block Size	**Overlapping Percentage**	**Precision**	**FPR**	**FNR**
5by 5	0%	94.21%	2.71%	24.85%
5 by 5	20%	96.57%	2.31%	20.02%
5 by 5	40%	95.65%	2.83%	14.67%
7 by 7	0%	96.81%	1.28%	33.37%
7 by 7	14%	**97.05%**	**1.11%**	**22.38%**
7 by 7	28%	96.80%	1.49%	20.76%
7 by 7	43%	96.67%	2.13%	17.60%

For further analysis, proposed method of bleeding zone detection is compared with recently developed method reported in [22]. In [22] bleeding localization is marked by fusion strategy of two stage-salient maps considering 0.8 weighting of first stage-salient. The comparison result of bleeding detection performance is illustrated in Table. 3.9. From the figure, it is clearly shown that the performance is significantly improved in terms of precision and FNR. Most important and significant improvement is observed in FNR ratio, it is improved by almost 16%.

Table 3.9: Performance Comparison of Bleeding Zone Detection

Method	**Precession**	**FPR**	**FNR**
Yuan method [22]	88.20%	3.14%	39.60%
R/G threshold	91.41%	6.23%	27.46%
Proposed Kmeans clustering	**97.05%**	**1.11%**	**22.38%**

Qualitative Analysis

For the purpose of qualitative analysis, four bleeding frames from four different patients videos is considered and presented in Fig. 3.10. The first column is the original image, while the second column shows the bleeding zone ground truth, the third column shows the detected bleeding region in the binary image and the final

column shows the bleeding zone in a color image. It is observed that proposed method successfully marked the bleeding zone. Also, it is clearly exhibited that bleeding zones are detected with high precision and accuracy, with some exception.

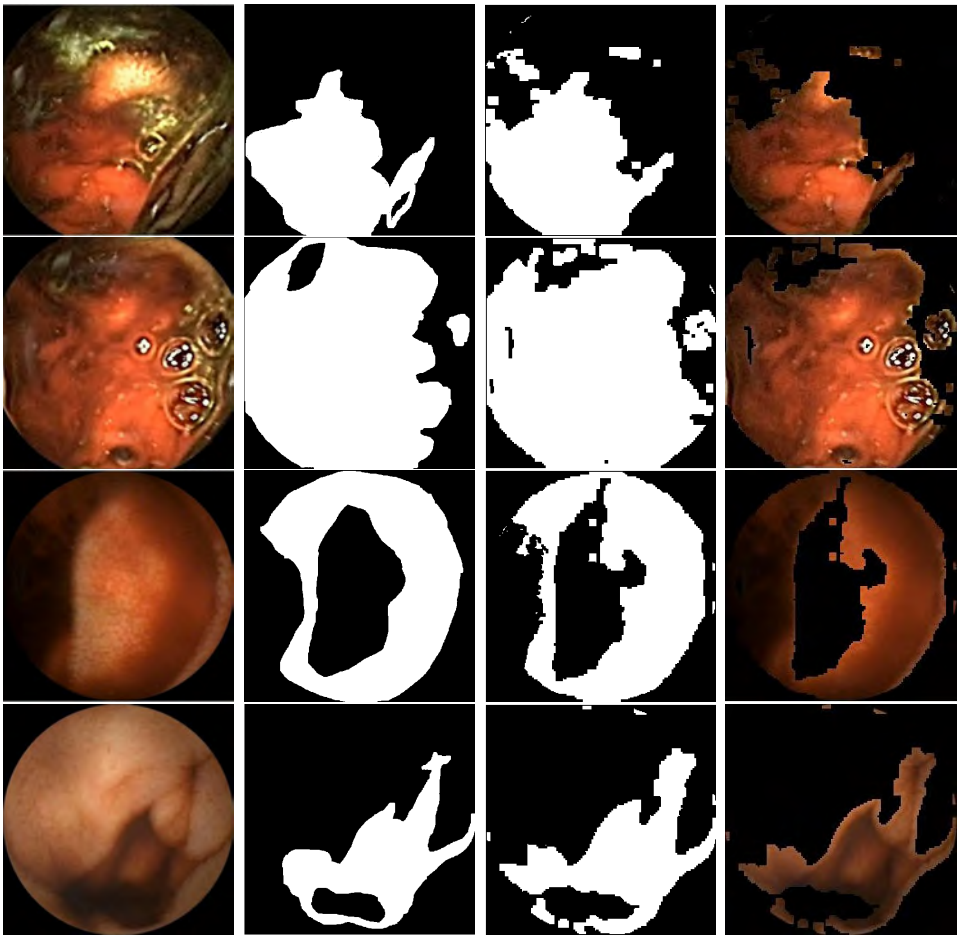

Fig. 3.10: Qualitative analysis of bleeding zone detection

3.5 Conclusion

In this chapter, a new technique of bleeding frame and zone detection in wireless capsule endoscopy video recordings is presented. The proposed method exhibits high sensitivity, specificity and accuracy with respect to other established method. In the proposed method, block base local feature extraction overcomes pixel randomness problem and provides consistent feature quality. Bleeding frame feature quality is enhanced by block clustering, especially in the case of small bleeding regions. And finally, global feature are extracted from the local feature, which offers computational efficiency. A novel post-processing algorithm is developed considering video frame sequence and global features, provides a significant improvement in perfor-

mance result. The extensive experiment demonstrates that medium block size with moderate block overlapping provides the best classification result. In the proposed method, the best result of bleeding frame detection is obtained from 7×7 with 14% overlapping block as sensitivity 95.47% and accuracy 96.64%. An automatic bleeding zone detection method is also presented with high precision. Bleeding zone detection method used previously obtain block cluster and pixel-wise marking are done by proposed interpolation technique. The proposed is thus promising in identifying bleeding zones from a bleeding image. In the future, we will develop more consistent and suitable feature for bleeding frame classification in order to archive the highest sensitivity.

Chapter 4

Proposed Color Histogram Based Bleeding Detection Scheme

In this chapter, an automatic bleeding image detection method is proposed utilizing construction of an index image incorporating a certain level of information from each plane of RGB color space. Distinguishable color texture feature is developed from index image by the histogram. Here, intensity values of all three available color planes are utilized thus called color histogram. A single pixel may be distorted due to the motion of capsule in GI tract. Hence, Instead of considering individual pixel values, a surrounding neighborhood block is chosen, from that block local statistical features are computed, hence global histogram feature is contracted using local features. From the observation of histogram pattern, an effective feature reduction scheme is proposed which minimize computational cost significantly without compromising performance. For the purpose of frame classification, the k-nearest neighbor (KNN) classifier is deployed. Satisfactory bleeding detection performance result is achieved in terms of accuracy, sensitivity, and specificity from severe experimentation on several WCE videos which are collected from a publicly available database. Moreover, for bleeding zone detection, blocks are classified using available local features, that do not incorporate any computational burden for feature extraction. It is noticed that proposed method successfully differentiate the bleeding areas from neighborhoods. Also, it is found that proposed method over performed with comparing some of the existing methods.

4.1 Introduction

The objective of this chapter is to develop an efficient computer aided bleeding frame and zone detection scheme in the WCE video recordings. A block-based local feature extraction is proposed from each color plane, which is more prominent representation instead of using individual pixel with respect to image noise, distortion, and bleeding zone. Color histogram based global features are extracted using each local feature. The final feature is formed by applying a proposed feature reduction scheme. For the purpose of bleeding and non-bleeding image classification a supervised k-nearest neighbor (KNN) classifier is proposed. Furthermore consecutive frames decision and final global feature are considered to develop a simple but effective post-processing scheme, to announce final bleeding frame of given WCE video recordings. This proposed post-processing step significantly improved bleeding frame detection performance. For the purpose of determining bleeding zone, the block is classified using available local features and pixel labeled within a block is determined with proposed interpolation method. Furthermore bleeding labeled pixel zone is fine-tuned by the morphological operation. Our main contributions can be summarized in the following three aspects.

- A color histogram based feature is proposed utilizing information of all three color planes
- A feature reduction scheme is developed, which significantly lessen computational cost without compromising performance
- A bleeding zone localization method is proposed using an available local feature of each block, that is not incorporated any computational burden in feature extraction process.

Work flow of the proposed method is illustrated in Fig. 4.1. Input of the proposed method is a WCE video segment, followed by preprocessing, feature extraction, feature dimenstion reduction, classification and post-processing. Output is the label of the frames (bleeding or non-bleeding), and detected bleeding zone of a bleeding image.

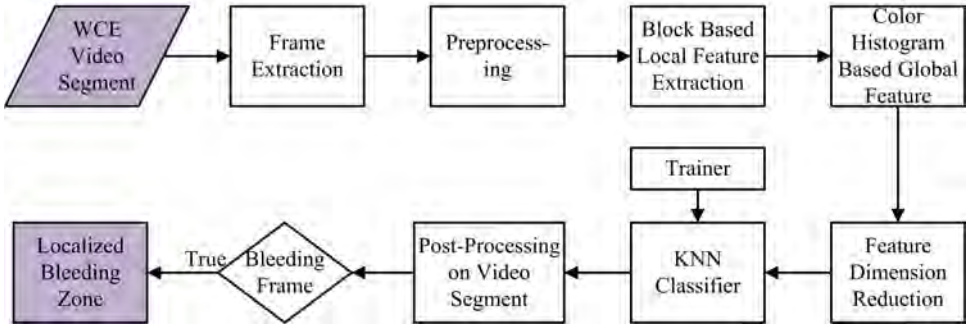

Fig. 4.1: Illustration of work flow of proposed method

4.2 Bleeding Frame Detection

4.2.1 Pixel Based Color Histogram (PChist)

A histogram measures the ratio of participation of different sub-classes in a given data. A color histogram is formed considering pixel intensity of all three color planes [39], [40]. Pixel intensities of all color planes are grouped together according to different ranges of their values (depending on bin size of the color histogram) and then the number of pixels in each group is counted. Let assume that all images contain the same number of blocks J. The color space of the image is discretized such that there are n distinct colors. A color histogram H_C can be defined as

$$H_C = \begin{bmatrix} h_1 & h_2 & h_3 & \cdots & h_n \end{bmatrix} \tag{4.1}$$

where each bucket h_j holds the number of blocks of color j in the image. Color histogram is widely used in comparing images and its popularity increased due to various aspects

- Color histograms are not affected by small fluctuations in camera viewpoint.
- Color histograms are computationally inexpensive.
- Distinctive color histogram often found for different objects.

Generally, WCE images are captured in the RGB color space and to acquire color histogram vector a few of the most significant bits (MSB) are utilized from each color plane. For example, in [37], three MSB bits are used for each color plane, thus, a total of $n = 512$ buckets histogram is formed.

In Fig. 4.2(a), three different planes are shown. Considering 8 bits separately, each one of the RGB planes can be considered as being composed of eight 1-bit

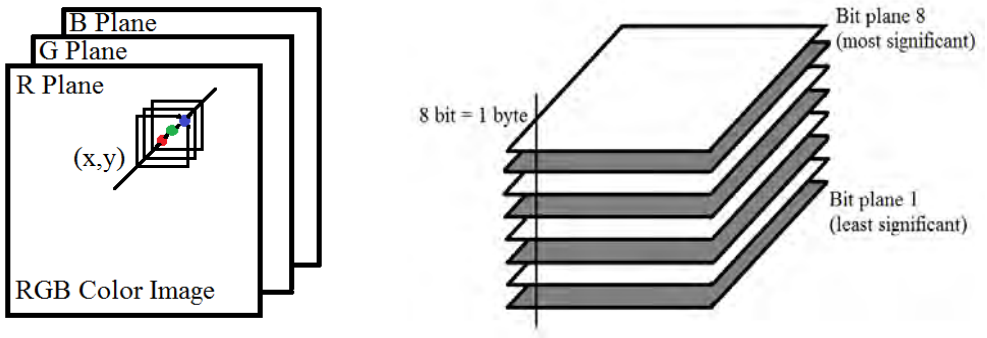

(a) (b)

Fig. 4.2: Indexed image construction from RGB planes: (a) Spatial marks for RGB color image; (b) Bit-plane representation of an 8-bit R color plane

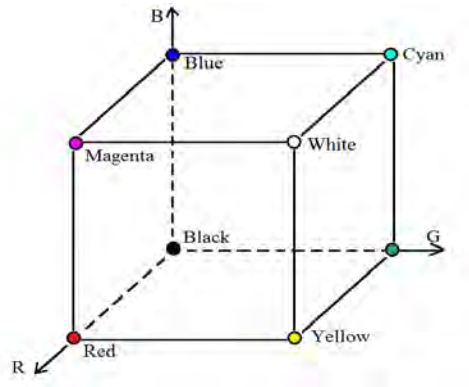

Fig. 4.3: Cartesian coordinate system of RGB color space

planes, which is demonstrated in Fig. 4.2(b). Here the eighth plane indicates the most significant bit (MSB) and the first plane indicates the least significant bit (LSB). Instead of considering all eight planes, one may consider only the MSB or two planes, MSB and the next one. For the purpose of classifying a block into one of the two classes, bleeding and non-bleeding, it is observed that use of eight planes (considering 256 different values for a pixel) may not be necessary and even makes the task difficult. If only one bit (MSB) plane is considered from each color plane, there will be total three bits from three planes and for each bit, there are two possibilities (0 and 1), resulting in $2^3 = 8$ different choices. As each pixel is now represented by three MSBs from three color planes, using Cartesian coordinate system, the color subspace of interest can be represented by a cube as shown in Fig. 4.3. As per the standard color scheme, eight colors obtained in this system are indicated in the figure. Use of the MSB of a color plane is, in fact, equivalent to considering normalized values 0 and 1 for each color space, where 0 represent the

intensity range 0 to 127 and 1 represent the intensity range 128 to 255. For each pixel, MSB information from all three planes is taken into consideration and the corresponding pixel is now assigned a new three-bit value. The given WCE image is now transformed into a different plane where the pixels are indexed with $3L$ bits where L indicates the number of bits (starting from MSB) to be considered for each color plane resulting in 2^{3L} combination for each block. For example, considering only MSB gives $L = 1$ and $2^3 = 8$ choices.

An index value is assigned for each color plane considering the binary value of the most L significant bits (MSBs). Let the index values are R_{ind}, G_{ind}, and B_{ind} corresponds to red, green and blue color planes. Final index value (F_{ind}) is calculated as the decimal values that corresponds to the binary choices

$$F_{ind} = 2^{2L} \times (R_{ind})_{10} + 2^{L} \times (G_{ind})_{10} + 2^{0} \times (B_{ind})_{10} \tag{4.2}$$

Here L is the number of MSB bits, which are taking into count. For example, when L=1 and mean of R, G, B planes of a block are $150, 180, 76$ respectively, then index value is [1 1 0] and final index, $F_{ind} = 2^2 \times 1 + 2^1 \times 1 + 2^0 \times 0 = 6$. To compute final index value, highest priority is given to red color plane due to its more prominent to bleeding. In order to capture spatial distribution of different colors, in the proposed scheme, combined color plane histogram approach is employed. Instead of considering the color distribution in one plane, information for constructing histogram is extracted from the index image plane described above. A color histogram represents the number of occurrence of each option of the index image. Formation of the index value is presented in Table. 4.1.

Table 4.1: Representation of Pixel Index Value

No.	**Pixel value (R,G,B)**	**1 bit (MSB)**			**Ind (0-7)**	**2 bit (MSB)**			**Ind (0-63)**
		R_{ind}	G_{ind}	B_{ind}		R_{ind}	G_{ind}	B_{ind}	
1	(100,230,50)	0	1	0	2	01	11	00	28
2	(150,240,30)	1	1	0	6	10	11	00	44
3	(50,60,10)	0	0	0	0	00	00	00	00
4	(200,120,100)	1	0	0	4	11	01	01	53
5	(240,235,250)	1	1	1	7	11	11	11	63

Color histogram, a count based representation of image pixels should ensure the presence of any group of bleeding pixels, no matter how small it is, independently in the feature vector. Thus, a color histogram is considered as more prominent and

significant representation of color in a given WCE image and it is to be noted that bleeding regions are sensitive to color information. In the case of small bleeding regions, it can provide discriminant feature value in the specific color bin, which is sufficient to detect the bleeding image. As a result, it is expected that the feature vector will offer better consistency no matter whether it is a bleeding or non-bleeding image. One of the major concern in the proposed method of global feature extraction is acquiring block based color histogram which is described below.

4.2.2 Block Based Feature Extraction

The motivation of block-based local feature extraction is described in section 3.2.1. In the previous chapter, block based method is developed using a composite color plane (G/R), which is a 2D plane, thus, the block is formed as a 2D block. Rather than a composite plane, in this chapter, all three available color planes are considered. It is to be mention that color images actually a data matrix of three dimensions. Two dimensions (X and Y axis) contain spatial information and the third dimension (Z axis) preserves color information. It is well known that color information plays a very significant role to differentiate bleeding and non-bleeding images. To represent a particular color, at least, three color planes information is required. To address this, all three color planes intensity information are considered to calculate local feature. Thus, in this section, a block is formed, which has three dimensions, consisted of both spatial and color planes information. For example,

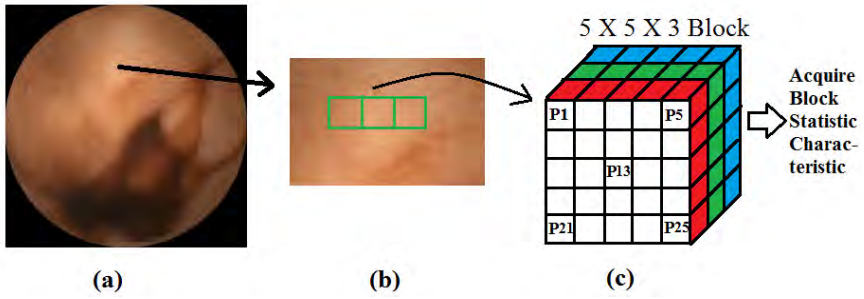

Fig. 4.4: Representation of neighborhood block characteristic (a) given image; (b) a representation of consecutive block; (c) block and statistic characteristics

considering a WCE color image with $M \times M$ pixels, and each pixel possesses value corresponding to C color planes (RGB color space, there are three color planes: R, G, and B), total dimension of that image becomes $M \times M \times C$. If pixel values are

directly considered as a feature, feature dimension would be $M \times M \times C$. However, if feature extraction is performed on $m \times m$ non-overlapping blocks in one channel, in total $J \times J$ blocks will be required, where $J = floor(M/m)$. In this case, if the average value of each color plane of each block is considered as a feature, $J \times J \times C$ average values containing local information can be used to construct feature vector with dimension $J^2 \times C < M^2 \times C$. It is to be mentioned that although only J^2 blocks instead of M^2 pixels are used in one channel, in each block all pixels are utilized to extract feature. Thus, conventional feature selection or pixel down-sampling operations are not equivalent to block based feature extraction. In Fig. 4.4, a block formation and local feature extraction method is illustrated. First, a given image is presented, then a block formation is presented from RGB color space (in this case a 5×5 spatial block is considered). In the figure, red, green and blue color represent each color plane. Finally, local features are computed separately for each color plane.

a pixel intensity becomes three dimensional vector and denoted as $\mathbf{p}(x, y, c)$ where $c = 1, 2, \cdots C$. For a block of size $m \times m$, pixel intensity of j-th pixel is denoted as $p_j(x, y, c)$, mean value of i-th block of each color plane are defined as

$$B^i_{mean}(c) = \frac{1}{m \times m} \sum_{j=1}^{m \times m} p_j(x, y, c) \tag{4.3}$$

where c is defined as color plane. Finally, block local feature of a statistical measurement is composed as

$$\mathbf{B}^i_{mean} = \begin{bmatrix} B^i_{mean}(1) & B^i_{mean}(2) & \dots & B^i_{mean}(C) \end{bmatrix} \tag{4.4}$$

Similar way, other conventional statistical measurements such as median, minimum and maximum of i-th block are computed

4.2.3 Proposed Block Feature Based Color Histogram

For the purpose of differentiating bleeding and non-bleeding images, a descriptive feature from a given WCE image needs to be extracted by employing features calculated from all blocks. For a given image, if all the extracted block features are combined, the feature vector would be tremendously large and it may not display a consistent pattern. One potential way out is to form a global feature for each

image by employing the features extracted from all blocks. If histogram from individual plane color is considered, that is not capable of characterizing bleeding pixels properly because to represent a single color, at least, three color channels are required [41]. Thus to represent bleeding, all color planes information are significant. In this circumstance, in order to find a suitable global feature, in this method, block based color histogram approach is proposed using all color planes intensity information [37].

The objective of this subsection is to present a scheme to extract a global feature of an image using available local features of each block. Instead of using one single color plane, statistical measures of all color planes are considered to extract global feature. For each local feature (e.g. mean, median, max, and min), a color histogram based global feature extraction method is proposed utilizing all blocks. At first, for a local feature, an index value is calculated using information of all color planes for each block. Similar to the case of pixel based color histogram as described in subsection 4.2.1. In this way, once index values of all blocks are computed, a histogram is contracted. Since the pixel value in RGB color space varies from 0 to 255, the value of the statistical measure of any block (e.g. mean, median, maximum, and minimum) will be confined within a range of 0 to 255. A color histogram of a bleeding image considering 1 bit MSB and the mean value of each block is constructed and represented in Table. 4.2. In that table, only MSB bit of each color space is considered, which results in 8 different classes.

Table 4.2: Representation of Color Histogram

Red	**Green**	**Blue**	**Color Index**	**Block Count**	**Block/Bin Probability**
0	0	0	0	744	0.327
0	0	1	1	0	0
0	1	0	2	0	0
0	1	1	3	0	0
1	0	0	4	626	0.275
1	0	1	5	0	0
1	1	0	6	805	0.354
1	1	1	7	100	0.044

For better understanding, considering the bleeding and non-bleeding images presented in Fig. 4.5 (a) and (b) respectively, eight bin histograms constructed from

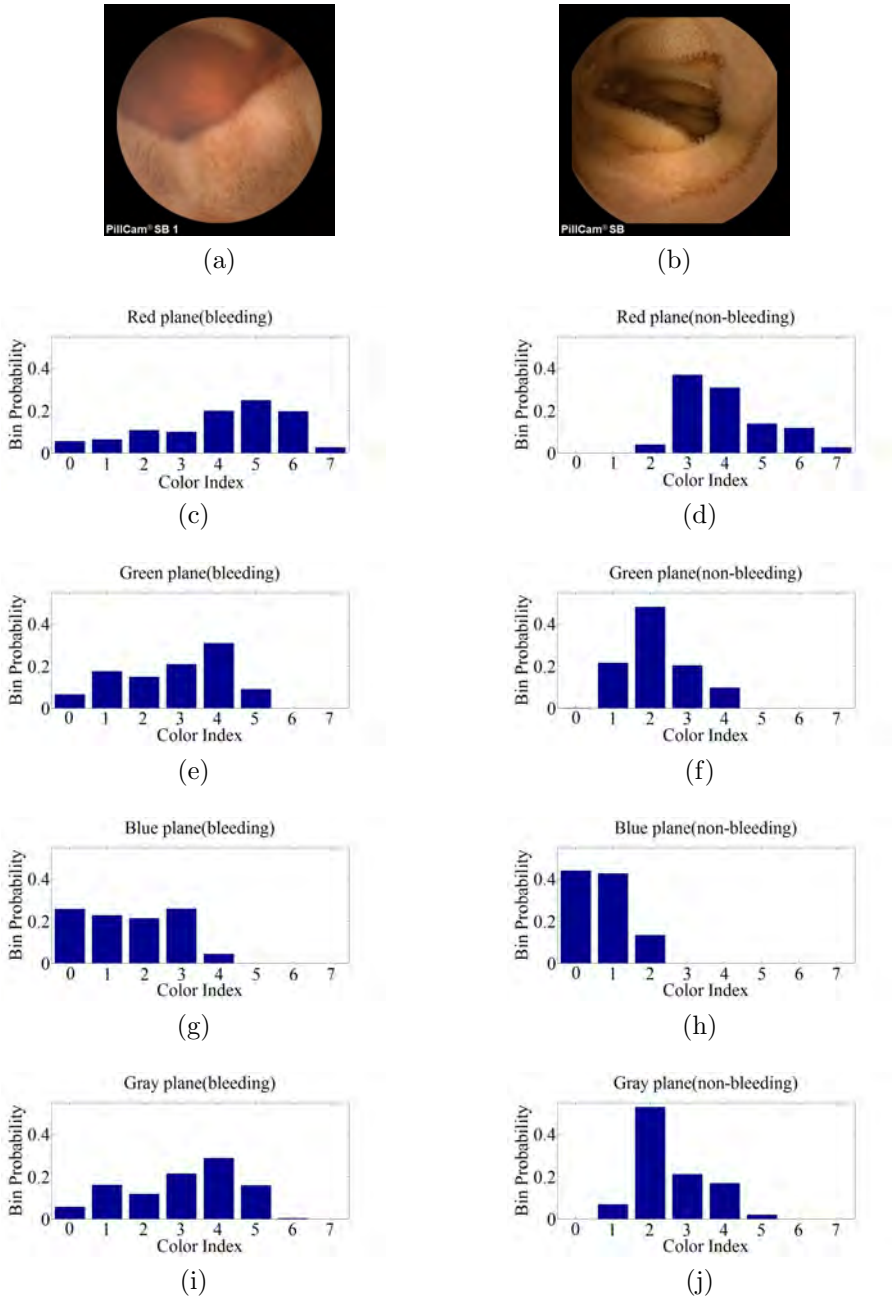

Fig. 4.5: Bleeding and non-bleeding image with individual plane color histogram, (a) bleeding image; (b) non-bleeding image; (c) R-plane (bleeding) histogram; (d) R-plane (non-bleeding) histogram; (e) G-plane (bleeding) histogram; (f) G-plane (non-bleeding) histogram; (g) B-plane (bleeding) histogram; (h) B-plane (non-bleeding) histogram; (i) gray image (bleeding) histogram; (j) gray image (non-bleeding) histogram.

different individual color planes are first shown in Fig. 4.5 (c)-(j). In this figure R, G, B three planes and the grayscale plane is shown separately. From the histogram figure, it is observed that bleeding and non-bleeding image exhibit quite similar histogram pattern with a large portion of overlapped regions between the two classes.

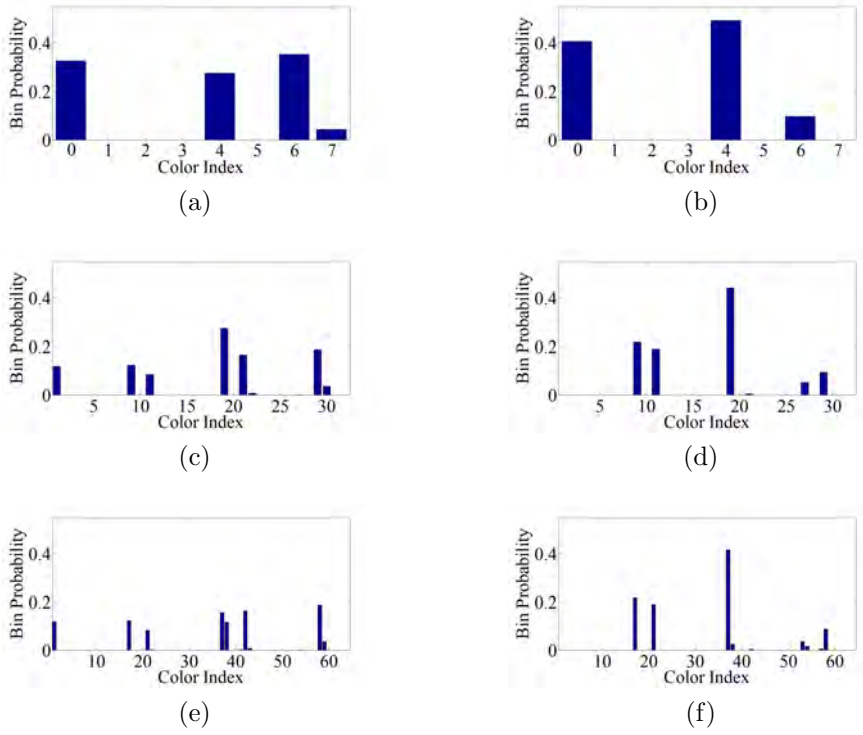

Fig. 4.6: Color histogram from proposed indexed image plane. 8 bin: (a) bleeding and (b) non-bleeding. 32 bin: (c) bleeding and (d) non-bleeding 64 bin: (e) bleeding and (f) non-bleeding.

Next in Fig. 4.6, for the same WCE images, histograms constructed from index image plane are shown considering 8, 32 and 64 bins. In Figs. 4.6 (a) and (b), 8 bin color histogram of bleeding and the non-bleeding image is illustrated respectively. Here, $L = 1$ is considered which gives $2^3 = 8$ index values and then 8 bin histogram is computed. For $L = 2$, $2^{3\times2} = 64$ index values can be acquired (local feature value of each plane is divided as 0 to 63, 64 to 127, 128 to 191 and 192 to 255 and represented by the most significant two bits (L = 2)), from that 32-bin color histogram is computed and presented in Figs. 4.6 (c) and (d). Similarly, 64-bin color histogram is shown in Figs. 4.6 (e) and (f). From the figure, it is observed that 8-bin color histogram shows distinguishable frequency in bin 4 and 6, 32-bin histogram shows very distinguishable frequency value in some of the bins (e.g. 0, 21, 27) and for 64-bin separability between the bleeding and non-bleeding image histogram is significantly increased with respect to 32-bin color histogram. It can be observed that the classification task is more difficult if the histogram of an individual plane (R, G, B, grayscale) is used. However, the histogram obtained by using index image offers better between class separation. Hence, a set of occurrence values of each color

in the index image histogram is proposed to be used as a potential global feature for classifying bleeding and non-bleeding images. In order to construct the feature vector, L bits (starting from MSB) of a pixel from each plane are taken and placed in a sequential manner to construct the transformed pixel value of the index image plane.

4.2.4 Feature Dimension Reduction Scheme

One of the major observations is made from the Table. 4.2 and the Figs. 4.5 (g) and (h) is that the blue intensity value in WCE image remains lower than 128 due to the inherent characteristics of GI tract. From the Table. 4.2, it is observed that pixel count is negligibly small or zero when the blue index value is 1, it is to be noted that index value 1 represents intensity range of 128-255. In Table 4.2, $B = 1$ corresponds to $1, 3, 5$, and 7 index values. In addition to this, from the Figs. 4.6 (a) and (b), it is observed that at color indices 1, 3, 5, and 7, bin probability is close to zero which do not make any sense to distinguish bleeding and non-bleeding frames. Thus, to reduce feature dimension, we propose to take only bin probability that contains blue intensity range 0-127. For example, in 8-bin color histogram, 0, 2, 4, and 6 colors index feature is proposed. Similarly for 64 bin, $0, 1, 4, 5, 8, 9 \cdots 60, 61$ color index feature is proposed. This approach reduces the feature dimension by 50% without mislaying any significant information regarding bleeding.

4.2.5 Effect of Feature Cascading

Bin probability of color histogram is constructed for each block based local feature (i.e. mean, median, minimum and maximum). In the simulation and result section, those color histogram features are tested and the block features that provide best performance result is proposed as final proposed feature. In addition to this, color histogram features constructed from different block features are cascaded to form a feature vector. The performance of those cascading features is presented in result and simulation section.

4.3 Bleeding Zone Localization

Once a bleeding image is detected in a WCE video, it is desired by the reviewer that bleeding zones are marked by the bleeding detection tools. Automatic bleeding zone localization can afford various assistances, namely 1) ratifying the bleeding recognition result of that image, 2) quick picturing of the region of importance intensively and 3) Exploring the variation in bleeding appearances in sequential video frames. But automatic bleeding zone localization facility is not offered in the most of existing bleeding recognition techniques. Thus in this section, a computer aided bleeding zone localization scheme is proposed, which is used for identifying bleeding regions in the detected bleeding frame. In the proposed method, first, local features are computed from different blocks, then using that local feature, the probability of each color histogram bins is computed and considered as a global feature and then feature based supervised classifier is used to identify bleeding (B) or non-bleeding (N) images. Next, bleeding zone localization will be performed only on bleeding images. At this point, the objective is to categorize the blocks of a given bleeding image into two classes as bleeding and non-bleeding block. After getting the block label, the label of a pixel in a block needs to be determined. And finally bleeding zone is localized using pixel-wise marking of a given image. Major steps, to be executed in the proposed bleeding zone localization procedure are as following

- Classify all the blocks of an image into bleeding and non-bleeding classes
- Identifying the label of each pixel in a block whether bleeding or non-bleeding
- Fine-tuning of bleeding zone with the help of morphology operation.

4.3.1 Block Classification

In order to classify blocks of a given bleeding image, available local features of each block are considered. It is to be mentioned that block based local features are already extracted for the purpose of bleeding frame detection and described in subsection 4.2.2. Any computational burden is not incorporated in feature extraction for the purpose of block classification because of using available local features of each block. Along with the block-based local features, the color intensity value of block center pixel of each color plane is included in the final feature vector. This block center

pixel intensity is a strong representative member of that block, which definitely enhances feature quality of a block in case of block classification.

$$\mathbf{f}_{block} = \begin{bmatrix} \mathbf{B}_{mean} & \mathbf{B}_{median} & \mathbf{B}_{max} & \mathbf{B}_{min} & I_c \end{bmatrix} \tag{4.5}$$

Here $\mathbf{f}_{block}$ and I_c represent the final block feature for classifier and color intensity value of block center pixel respectively. For the purpose of classification, a supervised KNN classifier is proposed and final block feature is considered as a feature vector. In KNN classifier, a training dataset consists by randomly chosen 20% bleeding images of the available database. Ground truth of bleeding localization of those bleeding images are denoted by an expert physician. Bleeding blocks are collected from the ground truth marking and considered as training dataset.

After that identifying the label of pixels is performed which is similar as described in section 3.3.2. Finally, fine-tuning of the bleeding zone using morphology operation is executed which is similar as described in section 2.2.1.

4.4 Simulation and Experimental Result

4.4.1 Parameter Selection

First, after applying preprocessing technique described in subsection 2.1.1, black-boundary pixels are eliminated from given WCE image. Next, for block-based local feature extraction, as described in subsection 4.2.2, different blocks are constructed and effect of variation of block size and percentage overlapped on bleeding detection performance is investigated. Performance evaluation result are reported considering four different block sizes: 3×3, 5×5 7×7 and 9×9 with various combinations of overlapping. Different local features, such as mean, median, maximum, and minimum are calculated. For the purpose of a global feature extraction color histogram is computed utilizing each block based local feature of all color space (refer to subsection 4.2.3. Block probability of histogram bin is considered as a global feature for each local feature. For bleeding frame classification KNN classifier is used. Experimental performance is evaluated based on 10 fold cross validation technique.

4.4.2 Bleeding Frame Detection Performance

Bleeding frame detection results of proposed method are reported in Table. 4.3 considering variation of different block sizes. 3×3, 5×5, 7×7 and 9×9 block dimensions are investigated taking block median of 512 bin histogram and found that, very small size of block could not represent a significant area of bleeding, on the other hand, big size of block may contain both bleeding and non-bleeding regions. As a result, it is more suitable to take the moderate size of the block to obtain the best performance result. Hence, better performance result is obtained for 7×7 block size. The performance of frame detection varying histogram bin is investigated and presented in Table. 4.4. 8, 16, 32, 64, 128, 256 and 512 bin histogram are examined, more than 512 bin is not considered due to avoid very large feature vector. Blocks are segmented into more classes by higher histogram bin which offers the most discriminant feature. Thus, better performance is obtained by higher order histogram bin. 512 and 256 histogram bin show satisfactory performance than other lower bin.

Table 4.3: The Effect of Block Size on Bleeding Frame Detection Performance

Block Size	**Sensitivity**	**Specificity**	**Accuracy**
3 by 3	93.58%	98.94%	97.91%
5 by 5	93.75%	98.90%	97.87%
7 by 7	**94.22%**	**99.22%**	**98.26%**
9 by 9	91.93%	98.38%	96.89%

Table 4.4: Performance of Bleeding Frame Detection Varying Histogram Bin

Block size	**Histogram Bin**	**Sensitivity**	**Specificity**	**Accuracy**
7 by 7	8	46.17%	87.42%	79.49%
	16	79.46%	95.89%	92.72%
	32	79.61%	95.95%	92.81%
	64	85.03%	96.79%	94.55%
	128	88.88%	98.36%	96.60%
	256	93.09%	98.74%	97.66%
	512	**94.22%**	**99.22%**	**98.26%**

Different types of overlapping blocks are investigated and reported in Table. 4.5. In that table, 7×7 block dimensions are considered due to their high-performance potential. 0%, 14%, 28% and 43% overlap between two consecutive blocks of 7×7 size

are taking into the investigation. More than 50% overlap between two consecutive blocks is not considered. It is observed that, overlapping block scheme is more suitable to overcome single pixel randomness and distortion problem, hence offers better feature consistency than non-overlapping block feature. Thus, overlapping block scheme performed better than a non-overlapping block. Performance result is also varied due to an overlapping percentage between adjacent blocks. In order to examine the effect of overlapping percentage between two adjacent blocks; 14%, 28% and 43% overlapping of 7×7 blocks are considered and found that, if a large portion of a block is overlapped, feature quality degraded as well as the performance. As a result, the best performance is obtained from 14% overlapping block of 7×7 size, which is shown in Table. 4.5.

Table 4.5: The Effect of Block Overlapping on Bleeding Frame Detection Performance

Block Size	**Overlapping Percentage**	**Sensitivity**	**Specificity**	**Accuracy**
7 by 7	0%	94.22%	99.22%	98.26%
	14%	**94.92%**	**99.23%**	**98.30%**
	28%	93.09%	99.11%	97.96%
	43%	93.84%	98.88%	97.91%

The performance variation effect of global feature constructed by different local features and their combination are tested and reported in Table. 4.6. It is found that from the individual local feature, the best performance obtained by block median value histogram of 512 bin. Among the different combination of local features, a combination of median and min shows the best performance in term of sensitivity and accuracy. 96.00% sensitivity and 98.72% accuracy are achieved using a combination of median and min histogram with 512 bin. The final proposed feature is the combination of median and minimum local features 512 bin color histogram of 7×7 block with 14% overlapping.

Furthermore, bleeding detection performance is investigated using different 'k' value of KNN classifier considering final proposed feature, which is illustrated in Fig. 4.7. From the figure, it is found that the best performance is obtained using $k = 2$ in terms of sensitivity, specificity, and accuracy. It is to be mentioned that one major contribution of this paper is the block based feature extraction. In order to

Table 4.6: Performance of Bleeding Frame Detection Varying Local feature of Block

Block Size	**Histogram Bin**	**Local Feature**	**Sen.**	**Spec.**	**Accu.**
7 by 7	512	Mean	94.22%	99.22%	98.26%
		Median	94.92%	99.23%	98.30%
		Maximum	94.04%	98.68%	97.87%
		Minimum	94.85%	99.06%	98.30%
		Mean, Median	94.44%	99.22%	98.30%
		Median, Min	**96.00%**	**99.47%**	**98.72%**
		Mean, Median, Max, Min	94.61%	99.48%	98.30%

demonstrate the effect of block based feature of proposed method, the comparison result between with and without block based approach is shown in Fig. 4.8. In the figure, bleeding detection performance in terms of sensitivity, specificity and accuracy are demonstrated considering without and with block based color histogram feature. Single pixel randomness and distortion problem are reduced by block based approach. Hence, it is expected that with block based feature provides better performance than without blocking. From the figure, it is clearly shown that blocking step significantly improves sensitivity, specificity, and accuracy, in the case of sensitivity, it is improved by approximately 2%.

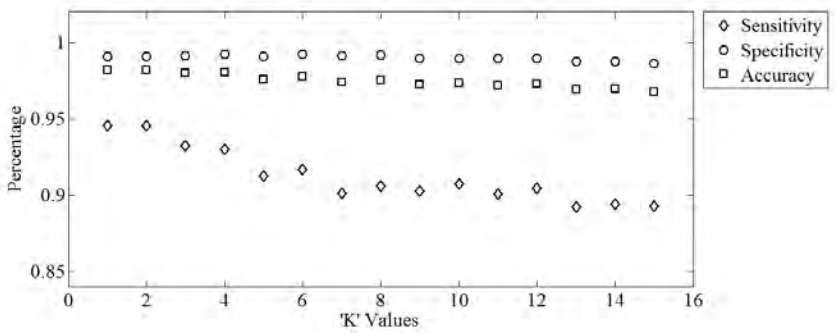

Fig. 4.7: Classification performance effect on 'K' values of KNN classifier

Although all the above results are reported in RGB color space, proposed feature extraction method is also tested among different color spaces like normalized RGB, HSV, CIElab, CIExyz, YCbCr and YIQ, which is illustrated in Fig. 4.9. In the figure, sensitivity, Specificity, and Accuracy are demonstrated considering above mentioned 7 color spaces and found that RGB and YIQ show highly satisfactory performance in term of all criteria. It is noted from the previous subsection, sensitivity is the most important performance criteria and high sensitivity is always desirable.

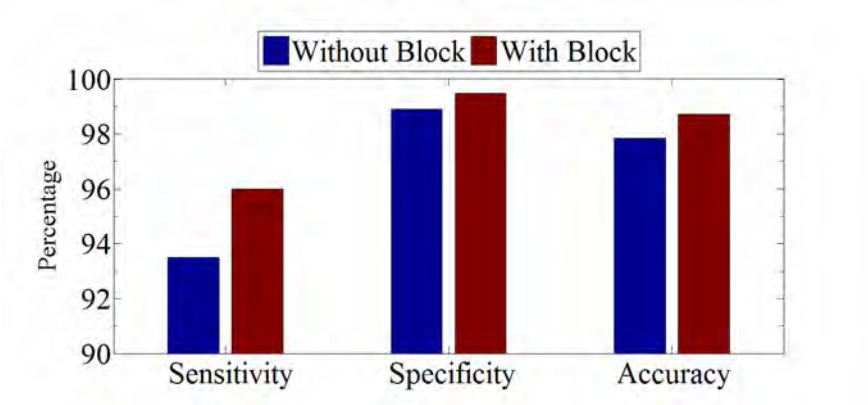

Fig. 4.8: Classification performance effect on block

Among the different color space, YIQ domain provides the best sensitivity in 256 bin color histogram. Finally, it is found that the best performance is obtained using 7×7 block size with 14% overlapping, along with a combination of 256 bin histogram of the median and minimum value of the block-based local feature in YIQ domain. To further evaluate the performance of proposed new method, it is compared with different histogram feature of RGB color space and reported in Table. 4.7. In the table, a block-based histogram of red (R) plane, green (G) plane, blue (B) plane and combination of all three color planes are taken into consideration. From the table, it is shown that our proposed block-based color histogram method perform better than any other histogram feature.

Table 4.7: Performance Comparison of Different Histogram Bin features of RGB Plane (%)

Block Size	**Histogram Feature**	**Feature Dimension**	**Sensitivity**	**Specificity**	**Accuracy**
7 by 7	R plane	256	84.13%	96.68%	94.26%
	G plane	256	79.04%	93.69%	90.89%
	B plane	256	74.14%	93.65%	89.79%
	Combined R, G, and B	768	94.50%	98.95%	98.06%
	Proposed Color Histogram	512	96.00%	99.47%	98.72%

Performance of Feature Dimension Reduction Scheme

One of the major contributions of this work is to reduce feature dimension by feature dimension reduction scheme (referred to subsection 4.2.4. This scheme offers a reduction of computational cost without compromising the performance. The perfor-

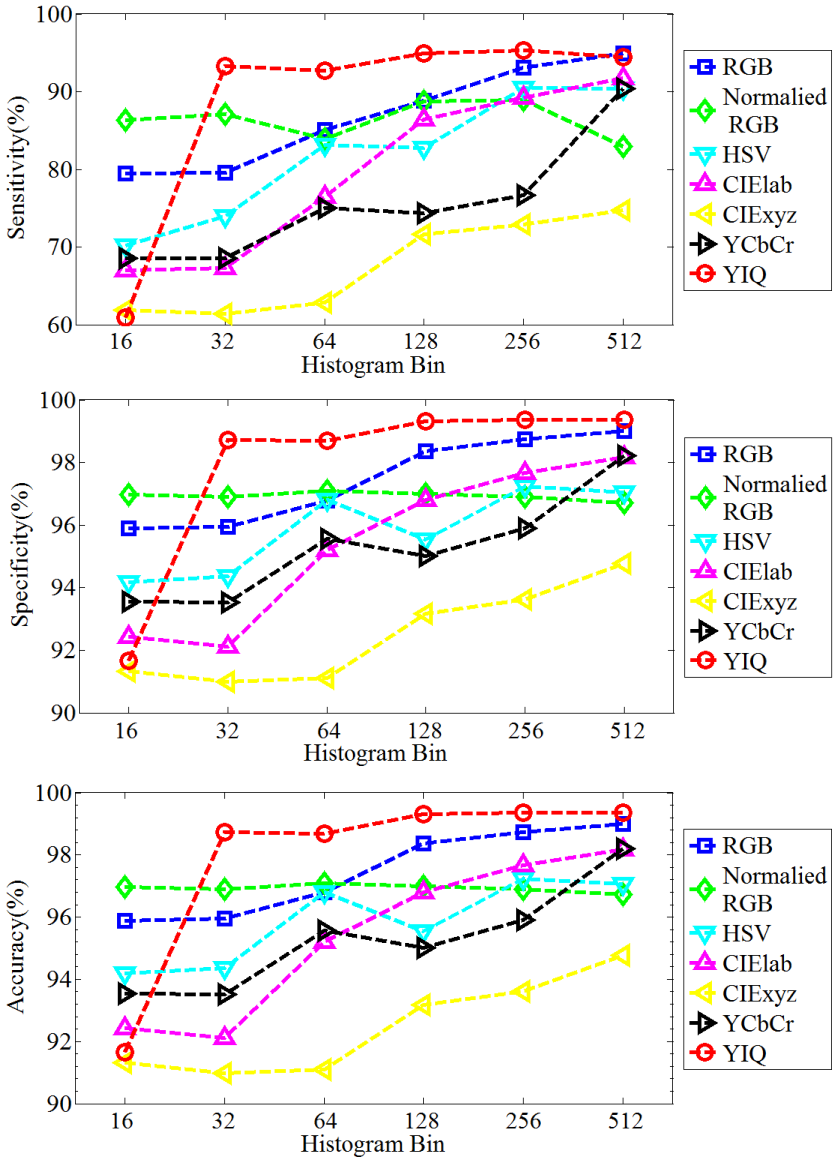

Fig. 4.9: Bleeding Detection Performance in Different Color Plane

mance comparison between with and without feature dimension reduction scheme is presented in Table. 4.8. From the table, it is found that feature dimension reduction scheme offers almost same performance while reducing feature size by 50%. It is to be noted that reduction of feature vector size significantly lessens the computational cost of classification.

Performance Comparison with Established Method

To further evaluate the performance of proposed method, it is compared with some recently established methods [23], [19], [32], [28], [27], [33], [34], [22] and [21]. At first proposed method is compared with uniformed Local Binary Pattern (LBP) his-

Table 4.8: Performance Comparison Between With and Without Feature Dimension Reduction Varying Histogram Bin

	Without Reduction				With Reduction			
Hist. Bin	**Dim.**	**Sen.**	**Spe.**	**Accu.**	**Dim.**	**Sen.**	**Spe.**	**Accu.**
32	32	79.61%	95.95%	92.81%	16	79.56%	95.73%	92.64%
64	64	85.03%	96.79%	94.55%	32	85.88%	96.53%	94.47%
128	128	88.88%	98.36%	96.60%	64	89.85%	98.42%	96.77%
256	256	93.09%	98.74%	97.66%	128	92.51%	98.59%	97.40%
512	512	94.22%	99.22%	98.26%	256	94.15%	99.15%	98.21%

togram feature. To extract feature in LBP, 8 bin histogram is performed. Other recent related papers, [19], [32], [37] and [22] focused on bleeding detection are considered for performance comparison, which is already mentioned in the introduction section. Best feature combination reported in [19] are taken into count. For [32], features are extracted from composite color intensity plane. A pixel intensity based color histogram feature of the whole image is taken for [37]. And for [22], 80 bin word based color histogram are considered as feature. The comparison result is reported in Table. 4.9. It is to be noted that in short proposed method is named as CH-BF (color histogram of block feature). For a fair comparison, same WCE image dataset and classifier are implemented. Our proposed method is developed in such a way that it can overcome some serious problem that usually WCE videos faces, like single pixel randomness, illumination changes, and image distortion. Also proposed method provides consistency feature not only for the image, that possess large bleeding zone but also for the image, that containing small bleeding zone. As a result proposed method shows the best performance result. From the table, it is exhibited that proposed method outperformed among the all reported methods, especially in terms of sensitivity.

4.4.3 Performance in Continuous WCE Video Clip

In this subsection, bleeding frame detection in continuous WCE video clip and the effect of post-processing step are demonstrated. For the purpose of analyzing performance in WCE video clip, five WCE bleeding videos are considered namely: 1) 'D170 bleeding', 2) 'bleding5', 3) 'bleeding3', 4) 'bleeding2', and 5) '23 bleeding', those are publicly available in [31]. Those videos are chosen in a way so that it

Table 4.9: Performance Comparison of Different Features

Method Name	**Sensitivity**	**Specificity**	**Accuracy**
Uniform LBP [23]	79.25%	94.56%	91.50%
Hist. probability [19]	83.00%	75.69%	77.15%
Intensity ratio [32]	94.78%	93.58%	94.00%
Stat (R/G) [28]	88.50%	96.63%	94.97%
Stat (Hue) [33]	93.08%	96.46%	95.24%
Stat (Y.I/Q) [34]	93.50%	94.00%	93.90%
Stat (CMYK) [27]	95.50%	92.87%	93.40%
Word hist. [22]	91.71%	94.05%	93.31%
Raw hist. [21]	94.50%	98.95%	98.06%
CCBF	96.22%	98.54%	98.04%
Proposed CH-BF	**96.09%**	**99.32%**	**98.68%**

covers different types of bleeding frame, as well as variation of frame number and position. First, from the video clip image frames are extracted and proposed final features are calculated. Then, bleeding and non-bleeding decision are acquired by applying KNN classifier and the performance is reported in Table. 4.10 and termed as without post-processing performance. Among the five videos, four videos show satisfactory performance in terms of all performance criteria, except 'bleeding3', due to the presence of numerous incidents of faint small bleeding areas. After getting primary bleeding detection result, post-processing algorithm is implemented. In The post-processing step, first, frame decision of video clip sequence is tested with certain conditions and acquired an investigation zone centering a frame which is primarily labeled as non-bleeding. Fulfilling necessary condition a test non-bleeding frame can be toggled to bleeding, which is described in 2.1.5. As a result, a bleeding frame decision may be corrected, thus, the sensitivity is improved. The performance result of with and without post-processing are reported in Table. 4.10 in terms of sensitivity, specificity, and accuracy. As expected, the sensitivity, as well as accuracy, is significantly improved by post processing. In the case of 'bleeding3' video, its sensitivity is highly improved as well as accuracy. The overall result of considering all five videos are illustrated in Fig. 4.10. From the figure, it is clearly shown that the overall sensitivity and accuracy are improved by almost 2% and 1% respectively, which reflects strong justification of post processing step.

Table 4.10: Video Performance Result with Post Processing Effect

Video name	**Frames No. (B/N)**	**Criteria**	**Without post-proc.**	**With post-proc.**
D170 bl	96/4	sen.	98.96%	100.00%
		spec.	75.00%	75.00%
		accu.	99.00%	99.00%
bleeding5	22/78	sen.	90.91%	95.45%
		spec.	96.15%	96.15%
		accu.	95.00%	96.00%
bleeding3	5/95	sen.	100.00%	100.00%
		spec.	89.47%	89.47%
		accu.	90.00%	90.00%
bleeding2	100/0	sen.	98.00%	100.00%
		spec.	—	—
		accu.	98.00%	100.00%
23 bl	27/73	sen.	81.48%	88.89%
		spec.	98.63%	98.63%
		accu.	94.00%	96.00%

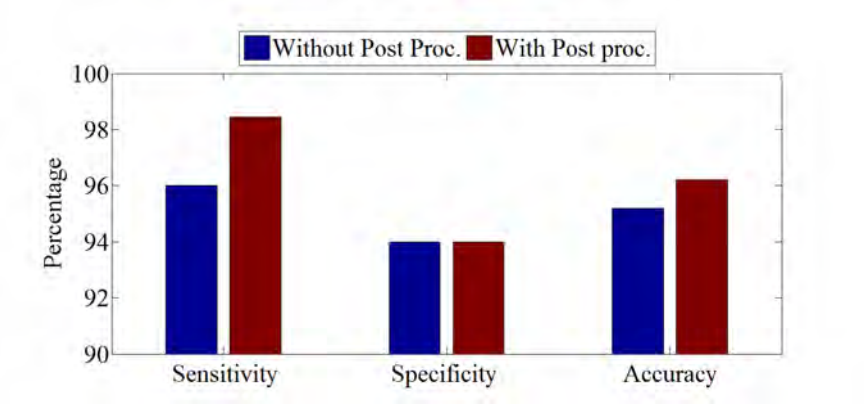

Fig. 4.10: Overall performance comparison between with and without post processing

4.4.4 Experiment Results for Bleeding Zone Detection

Quantitative Analysis

For the purpose of quantitative analysis, 100 bleeding images are tested, which are collected from 10 different bleeding videos. The ground truth of bleeding zone of those bleeding images is marked by the clinician. Bleeding zone detection result of a different parameter of proposed method are reported in Table. 4.11. Among the different performance parameters precession and the false negative ratio (FNR) is a more crucial indicator. According to the definition of precision, FPR, and FNR;

higher value is of precision but the lower value of FNR and FPR are considered as a good result. FNR value represents failure percentage of bleeding zone detection, which must be kept very low. As a result, high precision value and low FNR value are expected. Bleeding zone detection result of proposed method are reported in Table. 4.11 considering variation of different block sizes. 3×3, 5×5, 7×7 and 9×9 block dimensions are investigated and found that very small size of the block could not represent a significant area of bleeding, on the other hand, big size of the block may contain both bleeding and non-bleeding regions. As a result, it is more suitable to take the moderate size of the block to obtain the best performance result. Hence, in terms of precision, better performance result is obtained considering 7×7 block size. It is noted that bleeding zone detection performance highly depends on local block features, which are used for segmenting bleeding and non-bleeding zone as mentioned in 3.2.2.

Table 4.11: Bleeding Zone Detection Performance of Different Block Size

Method	**Precession**	**FPR**	**FNR**
3 by 3 block	94.28%	2.14%	8.46%
5 by 5 block	94.75%	4.01%	10.31%
7 by 7 block	**95.33%**	**3.14%**	**10.88%**
9 by 9 block	94.07%	1.34%	16.35%

Different types of overlapping blocks are investigated and reported in Table. 4.12. In that table, only 5×5, and 7×7 block dimensions are considered due to their high-performance potential. 0%, 20% and 40% overlap between two consecutive blocks of 5×5 size and 0%, 14%, 28% and 43% overlap between two consecutive blocks of 7×7 size are taking into the investigation. More than 50% overlap between two consecutive blocks is not considered. It is observed that, overlapping block scheme is more suitable to overcome single pixel randomness and distortion problem and offers consistent local block feature. Thus, overlapping block scheme performed better than a non-overlapping block. Performance result is also varied due to an overlapping percentage between adjacent blocks. In order to examine the effect of overlapping percentage between two adjacent blocks; 14%, 28% and 43% overlapping of 7×7 blocks are considered and found that, if a large portion of a block is overlapped, local feature quality of blocks are degraded as well as the bleeding zone detection performance. As a result, in terms of precision, the best performance

is obtained from 14% overlapping block of 7×7 size which is shown in Table. 4.12. To justify our methods, further analysis is done to compare bleeding zone detection result with recently developed method reported in [22] and other proposed methods. The comparison result of bleeding detection performance is illustrated in Table. 4.13. From the figure, it is clearly shown that all the performance parameters are significantly improved. Most important and significant improvement is observed in FNR ratio, it is improved by almost 29% from Yuan method. Proposed method performance is superior to both Yuan and R/G threshold-based method. Although, proposed method precession is lower than kmeans clustering method but it exhibits lower FNR, which is considered one of the very important performance parameter.

Table 4.12: The Effect of Block Overlapping on Bleeding Zone Detection Performance

Block Size	**Overlapping (%)**	**Precision**	**FPR**	**FNR**
7 by 7	0%	95.33%	3.14%	10.88%
7 by 7	14%	**95.75%**	**3.11%**	**10.38%**
7 by 7	28%	94.80%	3.49%	16.46%
7 by 7	43%	94.67%	4.13%	15.80%

Table 4.13: Performance Comparison of Bleeding Zone Detection

Method	**Precession**	**FPR**	**FNR**
Yuan method [22]	88.20%	3.14%	39.60%
R/G threshold	91.41%	6.23%	27.46%
Kmeans clustering	97.05%	1.11%	22.38%
Proposed block based classification	**95.75%**	**3.11%**	**10.38%**

4.5 Conclusion

In this chapter, a new technique of bleeding frame and zone detection in wireless capsule endoscopy video recordings is presented. In the proposed method, block base local feature extraction overcomes pixel randomness problem and provides consistent feature quality. The color histogram based global feature is proposed using the local feature. A feature reduction scheme is developed to reduce the computational cost of classification task without compromising the bleeding frame detection performance. The proposed method exhibits high sensitivity, specificity, and accuracy

with respect to other established method. Moreover, a bleeding zone localization method is developed using the local feature. First, blocks of a bleeding frame are classified using supervised classifier and then pixels are marked using proposed interpolation scheme. Finally, bleeding zones are delineated applying morphological operation. The proposed method is thus promising in identifying bleeding zones from a bleeding image. In the future, we will develop more consistent and suitable feature for bleeding frame classification in order to archive the highest sensitivity.

Chapter 5

Conclusion

5.1 Contribution of this Thesis

- The main objective of this thesis work is to develop a fast and efficient bleeding frame and zone detection technique for WCE video recordings. In order to achieve this target, three different schemes are proposed, one falls into the category of holistic-based approach, the second one is combination of block and segment based approach and the third one is color histogram based feature extraction approach. The objective of the first scheme is to provide satisfactory bleeding frame detection performance with a very low computational cost of processing the whole image. RGB color plane and a composite color plane based feature extraction method is developed and found that this method can successfully differentiate bleeding and non-bleeding WCE video frames. WCE video recording holds sequential information of frames, it is observed from the frame sequence that bleeding does not occur a discrete single frame rather than bleeding frames occur in a group of the continuous sequential frame. In this regard, a post-processing algorithm is developed to improve the performance of bleeding frame detection.

- A combination of block and segment based approach is introduced. This approach overcomes single pixel randomness problem as well as independent of the size of the bleeding area in a given image. A block-based local feature is extracted, which is considered more prominent representation instead of using individual pixel with respect to image noise, distortion, and bleeding zone. Furthermore, an unsupervised classifier is used to segment WCE image into two clusters, which separates bleeding blocks from non-bleeding blocks hence

enhance feature quality for detection of bleeding pixels.

- The third scheme proposed in this thesis performs 3D color histogram based bleeding and non-bleeding frame classification. A 3D color histogram is acquired utilizing information of all three color channels and the probability of bin frequency is proposed as a potential feature. This feature is considered as a good suit representation bleeding and non-bleeding pixel distribution in a given WCE image. One of the major contributions of this proposed scheme is a reduction of feature dimension, which significantly lessen computational cost without compromising performance.

- For the purpose of bleeding zone detection only bleeding marked images are taken into consideration. In this thesis, two approaches are developed for bleeding area localization. One approach uses clusters that are provided from the combination of block and segment-based approach. At first, from the two clusters (cluster-I and cluster-II) bleeding cluster is marked. Then pixel-wise marking is done by proposed interpolation technique and finally, with some morphological operation final bleeding zone is identified. Another approach to bleeding zone localization is a block-based classification of bleeding and non-bleeding zone. This approach also shows satisfactory performance result. Bleeding localization definitely helps the physician to diagnose bleeding source and as well as bleeding related abnormalities.

- The main objective of this thesis is to develop an efficient bleeding frame and bleeding zone detection methodology that can help the physician to diagnose bleeding related abnormalities. Our proposed method can successfully detect bleeding WCE video recording with a high level of sensitivity, specificity, and accuracy with respect to other recently publish method. Thus, it can reduce the burden of the physician in reviewing a large number of WCE images.

5.2 Scope & Future Work

- One possible future work could be to find more effective and distinguishable feature that is more prominent to differentiate bleeding and non-bleeding

frame. So that true bleeding image is not being misclassified as non-bleeding, this is very harmful in clinical aspect.

- Another future work could be to investigate not only bleeding abnormalities but also other diseases like tumor, ulcer etc. Then it will be a package for the user that any sort of abnormalities would be detected by computer aided system that definitely reduces the burden of the physician.

Bibliography

[1] U. C. Ghoshal, *Capsule Endoscopy: A New Era Of Gastrointestinal Endoscopy.* INTECH Open Access Publisher, 2013.

[2] G. Iddan, G. Meron, and A. Glukhovsky, "Wireless capsule endoscopy," *Nature*, vol. 405, pp. 417–417, 2000.

[3] A. Wang, S. Banerjee, and et al., "Wireless capsule endoscopy," *Gastrointest. Endosc.*, vol. 78, pp. 805–815, 2013.

[4] D. G. Adler and C. J. Gostout, "Wireless capsule endoscopy," *Hospital Physician*, pp. 14–22, 2003.

[5] (2014) Given imaging receives fda clearance for pillcam colon in patients following incomplete colonoscopy. [Online]. Available: http://www.givenimaging.com/enus/Innovative-Solutions/Capsule-Endoscopy/pillcam-colon/Pages/COLON-Pressrelease.aspx

[6] A. Moglia, A. Menciassi, P. Dario, and A. Cuschieri, "Capsule endoscopy: progress update and challenges ahead," *Nat Rev Gastroenterol Hepatol*, vol. 6, pp. 353–362, 2009.

[7] E. J. Carey and D. E. Fleischer, "Investigation of the small bowel in gastrointestinal bleeding–enteroscopy and capsule endoscopy," *Gastroenterol Clin North Am*, vol. 34, pp. 719–734, 2005.

[8] L. H. Lai, G. L. Wong, J. Y. Lau, J. J. Sung, and W. K. Leung, "Initial experience of real-time capsule endoscopy in monitoring progress of the videocapsule through the upper gi tract," *Gastrointest Endosc*, vol. 66, pp. 1211–1214, 2007.

[9] P. Valdastri, M. Simi, and W. R. J., "Advanced technologies for gastrointestinal endoscopy," *Annu. Rev. Biomed. Eng.*, vol. 14, pp. 397–429, 2012.

[10] L. B. Katz, "The role of surgery in occult gastrointestinal bleeding," *Seminars in gastrointestinal disease*, vol. 10, pp. 78–81, 1999.

[11] S. L. Triester, J. A. Leighton, and et al., "A meta-analysis of the yield of capsule endoscopy compared to other diagnostic modalities in patients with obscure gastrointestinal bleeding," *Am. J. Gastroenterol.*, vol. 100, pp. 2407–2418, 2005.

[12] ——, "Capsule endoscopy in the evaluation of patients with suspected small intestinal bleeding: Results of a pilot study," *Gastrointest. Endosc.*, vol. 56, pp. 349–353, 2002.

[13] W. A. Qureshi, "Current and future applications of the capsule camera," *Nat. Rev. drug Discov.*, vol. 3, pp. 447–450, 2004.

[14] J. M. e. a. Buscaglia, "Performance characteristics of the suspected blood indicator feature in capsule endoscopy according to indication for study," *Clinical gastroenterology and hepatology*, vol. 6, pp. 298–301, 2008.

[15] S. Liangpunsakul, L. Mays, and D. K. Rex, "Performance of given suspected blood indicator," *Americal Journal of Gastroenterology*, vol. 98, pp. 2676–78, 2003.

[16] C. Signorelli, F. Villa, E. Rondonotti, C. Abbiati, G. Beccari, and R. d. Franchis, "Sensitivity and specificity of the suspected blood identification system in video capsule enteroscopy," *Endoscopy*, vol. 37, pp. 1170–1173, 2005.

[17] G. Pan, G. Yan, X. Qiu, and J. Cui, "Bleeding detection in wireless capsule endoscopy based on probabilistic neural network," *J. Med. Syst.*, vol. 35, pp. 1477–84, 2011.

[18] M. Fu, Y.and Mandal and G. G., "Bleeding region detection in wce images based on colorfeatures and neural network," in *Proc. IEEE 54th Int'l Midwest Symposium on Circuits and Systems (MWSCAS)*, 2011, pp. 1–4.

[19] S. Sainju, F. M. Bui, and K. Wahid, "Bleeding detection in wireless capsule endoscopy based on color features from histogram probability," in *Proc. Canadian Conf. on Electrical and Computer Engineering, CCECE*, 2013, pp. 1–4.

[20] M. Ramaraj, S. Raghavan, V. Raghunath, and A. K. Wahid, "Histogram variance controlled bleeding detectors for wireless capsule endoscopic images," *Journal of Med. Imaging and Health Info.*, vol. 4, pp. 500–510, 2014.

[21] J. Liu and X. Yuan, "Obscure bleeding detection in endoscopy images using support vector machines," *Optimization and Engineering*, vol. 10, pp. 289–299, 2008.

[22] Y. Yuan, B. Li, and M. Q. H. Meng, "Bleeding frame and region detection in the wireless capsule endoscopy video," *IEEE Journal of Biomedical and Health Informatics*, vol. 19, pp. 1–7, 2015.

[23] B. Li and M. Q. H. Meng, "Computer-aided detection of bleeding regions for capsule endoscopy images," *IEEE Trans. Biomedical Engineering*, vol. 56, pp. 1032–39, 2009.

[24] Y. Lee and G. Yoon, "Real-time image analysis of capsule endoscopy for bleeding discrimination in embedded system platform," *World Acad. Sci. Eng. Technol.*, vol. 56, pp. 2526–2530, 2011.

[25] S. Sainju, F. M. Bui, and K. Wahid, "Automatic bleeding detection in wireless capsule endoscopy videos using statistical features and region growing," *Journal of Medical Systems*, vol. 38, pp. 1–11, 2014.

[26] Y. Fu, M. Mandal, and M. Q. H. Meng, "Computer-aided bleeding detection in wce video," *IEEE Journal of Biomedical and Health Informatics*, vol. 18, pp. 636–642, 2014.

[27] T. Ghosh, S. K. Bashar, S. A. Fattah, C. Shahnaz, and K. A. Wahid, "A feature extraction scheme from region of interest of wireless capsule endoscopy images for automatic bleeding detection," in *Proc. IEEE Symposium on Signal Processing and Information Technology ISSPIT*, 2014, pp. 1–4.

[28] T. Ghosh, S. K. Bashar, M. S. Alam, K. Wahid, and S. A. Fattah, "A statistical feature based novel method to detect bleeding in wireless capsule endoscopy images," in *Proc. Int'l Conf. on Informatics Electronics and Vision, ICIEV*, 2014, pp. 1–4.

[29] W. Gao, X. Zhang, L. Yang, and H. Liu, "An improved sobel edge detection," in *Proc. 3rd Int'l Conf. on Computer Science and Information Tech. (ICCSIT)*, 2010, pp. 67–71.

[30] D. G. Altman and J. M. Bland, "Diagnostic tests 1: Sensitivity and specificity," *Biomedical Journal*, vol. 308, p. 1552, 1994.

[31] (2014) The capsule endoscopy website. [Online]. Available: http://www.capsuleendoscopy.org

[32] T. Ghosh, K. Wahid, and S. A. Fattah, "Automatic bleeding detection in wireless capsule endoscopy based on rgb pixel intensity ratio," in *Proc. Int'l Conf. on Electrical Engineering and Information Commun. Techno., iCEEiCT*, 2014, pp. 1–4.

[33] T. Ghosh, S. K. Bashar, S. A. Fattah, C. Shahnaz, and K. A. Wahid, "An automatic bleeding detection scheme in wireless capsule endoscopy based on statistical features in hue space," in *Proc. Int'l Conf. on Computer and Information Technology ICCIT*, 2014, pp. 354–357.

[34] T. Ghosh, S. A. Fattah, S. K. Bashar, C. Shahnaz, K. A. Wahid, W. P. Zhu, and M. O. Ahmad, "An automatic bleeding detection technique in wireless capsule endoscopy from region of interest," in *Proc. IEEE Int'l Conf. on Digital Signal Processing DSP*, 2015, pp. 1293–1297.

[35] F. Conversano, R. Franchini, C. Demitri, L. Massoptier, and M. A. et al., "Hepatic vessel segmentation for $3d$ planning of liver surgery: experimental evaluation of a new fully automatic algorithm," *Academic radiology*, vol. 18, pp. 461–470, 2011.

[36] F. Conversano, E. Casciaro, R. Franchini, S. Casciaro, and A. Lay-Ekuakille, "Fully automatic $3d$ segmentation measurements of human liver vessels from contrast-enhanced ct," in *Proc. IEEE Medical Measurements and Applications MeMeA*, 2014, pp. 1–5.

[37] T. Ghosh, S. A. Fattah, C. Shahnaz, and K. A. Wahid, "An automatic bleeding detection scheme in wireless capsule endoscopy based histogram of an rgb-

indexed image," in *Proc. IEEE Engineering in Medicine and Biology Society EBMC*, 2014, pp. 4683–4686.

[38] W. F. Young, P. M. Valero-Mora, and M. Friendly, *Visual Statistics: Seeing Data with Dynamic Interactive Graphics*. Hoboken, New Jersey: John Wiley and Sons, Inc., 2006.

[39] J. Hafner, H. S. Sawhney, W. Equitz, M. Flickner, and W. Niblack, "Efficient color histogram indexing for quadratic form distance functions," *Pattern Analysis and Machine Intelligence, IEEE Transactions on*, vol. 17, pp. 729–736, 1995.

[40] M. Stricker and M. Swain, "The capacity of color histogram indexing," in *Computer Vision and Pattern Recognition, 1994. Proceedings CVPR'94., 1994 IEEE Computer Society Conference on*. IEEE, 1994, pp. 704–708.

[41] K. N. Plataniotis and A. N. Venetsanopoulos, *Color Image Processing and Applications*. New York, USA: Springer-Verlag, 2000.